POLITECNICO
MILANO 1863

SCUOLA DI INGEGNERIA INDUSTRIALE
E DELL'INFORMAZIONE

3D Bioprinting of vascular structures for organoids models

TESI MAGISTRALE IN BIOMEDICAL ENGINEERING

Guiducci, Camilla, 10556798

Advisor:
Gabriele Angelo Dubini

Co-advisors:
Alessandro Filippo Maria Pellegata

Academic year:
2021-22

Abstract: Organoids, 3D multicellular structures that mimic the architecture and functionality of a specific organ *in vivo*, are increasingly taking ground in biomedical research as novel human-specific *in vitro* models. However, the lack of a vasculature prevents them from reaching a full functionality and from a long-term survival. Although *in vitro* organoid vascularization has been attempted by numerous different strategies, to date none of them has been demonstrated to achieve a fully perfusable vascular system. The present study addresses this issue through the 3D bioprinting of an endothelial cells-laden bioink aiming to create a vascular structure for colon organoid perfusion. In particular, this work has focused on the optimization of the network bioprinting process, allowing to define the suitable printing parameters as well as the geometry of the network designed to host colon organoids, but also that of the internal structures printed right inside the lattice. G-codes modifications enabled to print both the inner and the outer structures without damaging each other, along with the bioprinting of multiple constructs in a muti-well plate. Moreover, the choice of the proper nozzle and bioink, together with the optimization of the bioprinting protocol, allowed to print high-resolution constructs, which did not dissolve in culture medium enabling endothelial cells proliferation and survival as well as the seeding of colon epithelial cells.

Key-words: 3D bioprinting, organoids, vascularization, colon, endothelial cells, bioink

1. Introduction

Recently great efforts have been made to develop *in vitro* models that allow the modelling of human tissues. *In vitro* models of human tissues are in fact becoming pivotal for personalised medicine, drug testing, innovative therapies testing (i.e., gene therapy) and modelling of human development [1].

Research on the mechanisms behind the formation, function and pathology of tissues and organs is mainly due to the use of cell culture systems and animal models [2]. Over the past 30 years, the use of both of them has led to a great progress in the comprehension of human development and

mechanisms of disease, but it has also highlighted the limits of these systems in mimicking human pathophysiology [3].

Cell culture is a widely used *in vitro* tool for improving our knowledge of cell biology, tissue morphology and mechanisms of diseases, drug action, protein production, as well as for the development of tissue engineering and above all for modelling human development and diseases [1]. The advantages of 2D cultures, such as simple and low-cost maintenance of the cell culture and the performance of functional tests, have made them largely adopted in many biomedical studies. Despite this, conventional monolayer cell cultures fail to inform the true biological processes *in vivo* because of the lack of tissue architecture and complexity of such models. 2D cultured cells in fact cannot mimic properly the natural structures of tissues and neither cell-cell and cell-extracellular environment interactions, which are responsible for cell differentiation, proliferation, vitality, expression of genes and proteins, responsiveness to stimuli, drug metabolism and other cellular functions[2]. As a consequence, 2D conditions alter cell morphology, polarity and mode of division and can cause the loss of diverse phenotype. An altered cell morphology can affect cell function, the organization of the structures inside the cell, secretion and cell signalling.

Furthermore, cells in the monolayer have unlimited access to the ingredients of the medium, such as oxygen, nutrients, metabolites and signal molecules, while cells *in vivo* can dispose of a variable quantitative of such components according to the natural architecture of the tissues [2]. Another drawback of 2D cultures is that, being usually monocultures, they allow the study of only one cell type, while all the tissues are made up of different cell types. These disadvantages led to the need of alternative models which better emulate natural tissues, such as 3D culture systems.

On the other hand, animal models have been an inestimable tool for the understanding of human biology and disease, thanks to the common principles of animal development and organ physiology. Among mammalian model systems, murine models are the most used for research studies, nevertheless, they do not properly recapitulate humans and so they often do not provide human-like results. Although humans have many similarities with mice and rats, especially at the genetic level, some important differences between murine and human physiology prevent some results achieved on murine models from being transferred to humans, as evidenced by the failure of many clinical trials [3]. This has become a major limit in the drug discovery process. Moreover, some biological processes are specific to the human body and cannot be modelled in other animals, such as brain development, metabolism and the testing of drug efficacy. Understanding human genetic diversity and its influence on disease onset and progression as well as on drug responses is fundamental for developing personalized medical treatments, but the creation of human-specific model systems is mandatory for this to happen.

1.1 Organoids

In order to overcome the limitations of all these models, many attempts to model human tissues and organs have been made and have shown some potential for drug screening or human disease research, but the human *in vitro* 3D cell culture approaches that are increasingly gaining ground are the so called 'organoids' [3].

They are 3D self-organizing multicellular structures mimicking the architecture, cellular heterogeneity and functionality of an organ *in vivo* [1]. They can be generated from human Embryonic Stem Cells (hESCs), human induced Pluripotent Stem Cells (hiPSCs) or Adult Stem Cells (ASCs) by recapitulating human development or organ regeneration *in vitro* [3]. In fact, through

guided differentiation protocols that resemble organogenesis, stem cells are driven to cell differentiation into organ-specific cell types and in 3D tissue assembly [4].

The 3D structure of organoids can be obtained by suspension culture using scaffold or scaffold-free techniques. Scaffolds can be synthetic or biological hydrogels resembling the natural ECM [1]. The most used is Matrigel, a gelatinous protein mixture derived from mouse tumour cells, which provides ECM signals and a bearing structure to the cells promoting cell proliferation and differentiation [5]. As a regard for scaffold-free techniques, cells can be cultured in suspension in droplets of culture medium or via "air-liquid-interface".

Intestinal organoids for example, recapitulating the intestinal architecture and physiology (Figure 1.1), are 3D structures consisting of crypts and villi, in which all the different intestinal cell types are present and spatially distributed exactly as in the intestine. In fact, Enterocytes, Goblet cells and Entereoendocrine cells are located in the villus-like domains, while intestinal stem cells (ISCs) Lgr5+ (Leu-rich repeat-containing G protein-coupled receptor 5) and Paneth cells reside in the crypt-like domains. In particular, self-organizing and self-renewing ISCs migrate from the depth of the crypt to the upper part differentiating in all the different intestinal cell types and thus contributing to the tissue homeostasis [6].

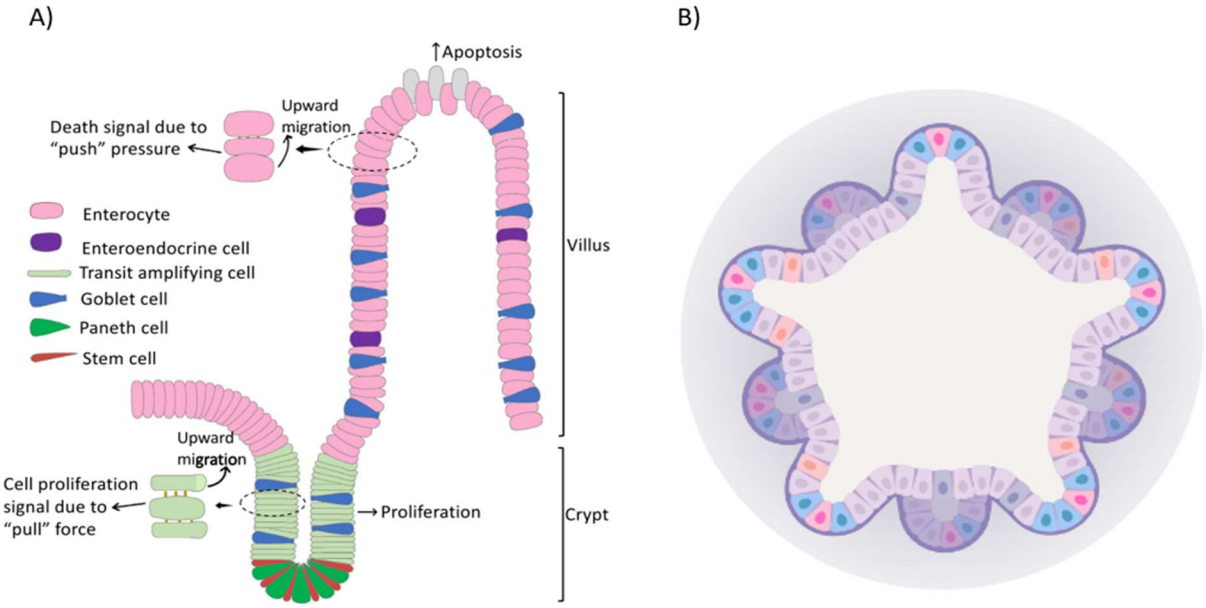

Figure 1.1 Schematic illustration of intestinal crypts and villi (A) and of an intestinal organoid (B)

Enterocytes actively control the adsorption of substances from the lumen to the submucosa, Goblet cells secrete mucous lubricating the digested material, Enteroendocrine cells are responsible for production and release of a series of hormones and Paneth cells produce proteolytic enzymes. The presence of all these cell types makes intestinal organoids capable of better imitating not only the architecture, but also the intestinal functionality. They, thus, hold a huge potential for the study of intestinal development, biology and pathophysiology [7].

Organoids represent a powerful new technology for many biological and clinical applications (Figure 1.2) [8]. They can be used to study organ development, biology and pathophysiology, but also for disease modelling to investigate infectious diseases, degenerative diseases, genetic disorders and cancers [3]. They also provide a promising new tool for regenerative medicine and, in

combination with editing technology, for gene therapy. Furthermore, patient-derived organoids can be exploited for personalized medicine and drug screening to predict the patient-specific drug response [7]. But there are also further applications, such as biobanking, toxicology studies, drug discovery studies, host-microbiome interactions, multiomics and phylogenetic studies [1].

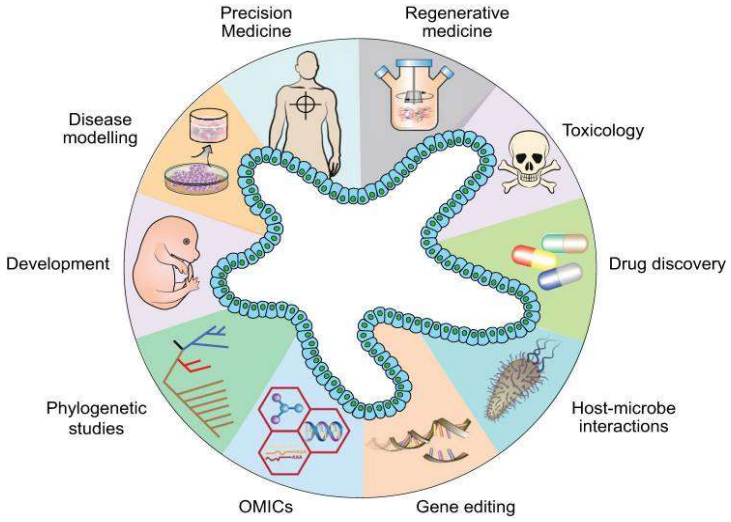

Figure 1.2 Schematic diagram of organoids applications [1]

Although organoids show a great potential as *in vitro* models, there are still many limitations to overcome. In fact, most organoids are suspended in Matrigel, an ECM derived from mouse sarcoma, which prevents their clinical use and whose properties may affect organoid cultures. Moreover, culture media usually contain plenty of growth factors, which could alter the natural morphogen gradients of the tissues. Another drawback is the ineffectiveness to reproduce the microenvironment, which consists of endothelial cells, fibroblasts, immune cells and ECM, and this might prevent the prediction of clinical outcomes. Furthermore, some practical troubles hinder the translation to clinical use, such as the high reagent cost for organoids fabrication, the complexity of 3D culture systems and the standardization of drug screening strategies [1].

1.2 Vascularization

One of the main limitations of organoids is, however, the lack of a vascularization system. In order to enhance the organ biomimicry, all the components that make up the organ must be replicated and, thus, also the vascular network. This is not just an anatomical part of the organ, but it also plays a key role in organ functionality. In fact, just like in the *in vivo* organs, blood vessels are responsible for supplying cells with oxygen and nutrients and for catabolites dumping, and so they are in charge of organoid vitality [9].

Organoids are 3D structures of the order of mm, however oxygen can only diffuse for a distance of 200-300 microns and so it can at most reach the outermost cells. Organoids must be perfused, otherwise inner cells will quickly die giving rise to a necrotic core [10]. Hence the need of a vascularization system, which might increase the overall size and life span of organoids and improve their maturation beyond the embryonic and fetal phase [4], [11].

Many attempts to vascularize organoids have been made, however at present the only method that has been demonstrated to successfully achieve a perfusable vasculature within organoid is the *in*

vivo transplantation into host animals in highly vascularized regions, where the host vasculature invades the organoid mimicking the angiogenesis *in vivo* [4], [11]. This approach allows organoids to develop a functional tissue architecture, improving their survival and maturation. Nevertheless, the need to experiment on animal models poses a paradox, since one of the main goals is to create human-specific models [12].

Furthermore, the organoid *in vitro* pre-vascularization before transplantation has been proven to enhance organoids survival and maturation, highlighting the importance of functional vasculature through the anastomosis between host and organoid vessels. Pre-vascularization, thus, could be crucial for developing a fully perfusable organoid *in vitro* platform [4].

There are different strategies to pre-vascularize organoids *in vitro*: co-colture of organoids with endothelial cells (ECs), co-differentiation with mesodermal progenitor cells, and mechanical stimulation, subjecting organoids to continuous media flow in microfluidic devices improving the development of a functional vasculature [4], [10].

Although these *in vitro* methods allow to achieve various degree of vascularization, none of them has led to a fully intravascular perfusion within organoid without *in vivo* transplantation, so organoids cannot be considered as truly vascularized *in vitro* yet [4], [12].

In order to achieve functional intravascular perfusion within organoids, anastomosis between internal vasculature and external vessels in the surrounding ECM is mandatory and this can be fulfilled trough engineering of perfusable *in vitro* capillary beds that provide suitable *in vitro* platforms to grow pre-vascularized organoids [4]. The techniques for engineering *in vitro* vascular beds can be classified into self-organized and pre-patterned methods [11].

The self-organizing approach relies on promoting vasculogenesis or angiogenesis, leading to spontaneous formation of vessels by ECs in hydrogels. *In vitro* vasculogenesis models use microfluidic platforms filled with hydrogels seeded with ECs that self-organize into capillaries leading to a perfusable network. *In vitro* angiogenesis models involve seeding EC monolayers onto the surface of hydrogels, which are integrated in microfluidics where tip cell migration and vessels formation across the gel can occur, leading to a functional vascular bed [4]. Seeding organoids into the microfluidic device leads to their vascularization through ECs sprouting into the gel. Self-organized vascular networks mimic *in vivo* capillaries in both morphology and function, but the geometry of spontaneously formed vasculature cannot be pre-defined and, thus, it's not reproducible [11].

Conversely, functional vascular beds with pre-defined geometries can be realized through different pre-patterning techniques, classified into subtractive and additive approaches. The subtractive approach involves building a network of 3D channels within a hydrogel by casting cell-laden hydrogels around a sacrificial mold, which is dissolved or removed afterwards leaving hollow channels for perfusion, where ECs are then seeded to generate a monolayer on the channel walls [12]. On the other hand, the additive approach consists in bioprinting a micro-fibrous scaffold using bioinks that contain ECs, which then gradually migrate toward the periphery of the microfibers generating a layer of confluent endothelium. Tissue-specific cells are then seeded into the interstitial space of the endothelialized scaffold to generate an *in vitro* vascularized tissue [11]. Unlike the self-organizing approach, pre-patterning techniques allow to control the geometry of vascular beds, however vessels diameter is usually larger than that of a *in vivo* capillary, due to physical limitations of the materials for temporary mold, the size of bioprinting nozzles and the difficulties of inducing ECs to migrate into small holes [4].

Next step is the integration of pre-vascularized organoids with *in vitro* capillary beds to create a fully perfusable system. However, the main outstanding challenge lies in generating functional anastomoses between organoids and vascular beds. This can be obtained with an 'inside-out' approach, that depends on expansion and outgrowth of organoid vasculature into surrounding ECM and anastomosis with bed vessels. Otherwise, an 'outside-in' approach can be used, inducing angiogenic sprouts from ECs making up the vascular bed to penetrate into the organoids and connect with their vessels [4] .

Though some of the strategies described have achieved promising results in vascularized tissue models, bioprinting represents nowadays the cutting-edge biofabrication technology in the field for its precise control over the structure of the fabricated constructs and the spatial distribution of cells, as well as for its cost-effectiveness and versatility [12], [13].

1.3 3D Bioprinting

3D bioprinting is an additive manufacturing technology by which 3D solid objects are made from a digital model through a layer-by-layer deposition of bioinks, which consist of natural or synthetic biomaterials that can be mixed with living cells [14], [15].

This technology allows the manufacture of complex geometries by following a CAD design of the structure to be printed, from which a STL file is generated [16]. Then a slicing software slices the 3D model and automatically generates a G-code file, which contains the coordinates along which the 3D printer moves dispensing the bioink in the desired 3D pattern [17] .

There are three main 3D bioprinting strategies. Inkjet-based bioprinting relies on the production of bioink droplets by generating bubbles in the tip of the printer through thermal, piezoelectric or acoustic energy [12]. Laser-assisted bioprinting is also based on the generation of bioink droplets by focusing a laser beam on an energy absorbing layer coupled with a donor-slide made up of bioink, the droplets are then deposited on a receiving substrate [15]. In extrusion-based bioprinting the bioink is pressed through the nozzle either with a piston, a screw or using pneumatic pressure and it is deposited as a continuous filament onto a flat substrate [18].

Extrusion is the most commonly used method. Compared to other techniques, it has a higher printing speed and many bioinks with a quite wide range of viscosity can be used. Moreover, the continuous deposition of filaments allows a greater structural integrity and this technology can be easily combined with CAD software. Cell viability ranges from 40% to 90%, but with the optimization of printing parameters, such as deposition rate, pressure and temperature, it can reach 97% with bioinks such as GelMA. Furthermore, this technology has a relatively poor resolution, with 100 μm as the optimal, which strictly depends on the nozzle size: the smaller is the size, the higher is the resolution, but also the shear stress that may damage the living cells and so the lower is cell viability [18]. A compromise between resolution and cell viability must be found.

Among the different extrusion strategies, pneumatic dispensing in the most used one, but some critical parameters must be considered: bioink rheological properties, extrusion temperature, applied pressure and nozzle size. For a good printability and print fidelity bioink viscosity must allow smooth nozzle extrusion, but at the same time it must be sufficiently high to allow the bioink extrusion in the form of a continuous filament instead of droplets, but also to avoid filament expansion after deposition and thus shape loss or construct collapse. However, an excessive viscosity can cause nozzle clogging. Additionally, a high yield stress, a shear thinning behaviour and a quick recovery kinetics to allow a fast solidification after printing are essential [9]. Last but not

least, bioink viscosity also affects the mechanical properties of the final construct as well as cellular viability and behaviour (proliferation, differentiation, migration, etc.) [12].

Moreover, it must be considered that also reproducibility is influenced by the same parameters, namely, nozzle diameter, pressure, printing speed, temperature and humidity, and it should not be forgotten thar they all affect also cell behaviour and viability [15].

The design of the 3D digital model requires to consider a few critical parameters. First, the ideal dimensions of the model could be affected by the slicing process that slices the model in multiple layers of a certain height, resulting in an altered height of the real printed structure. Also the filament extrusion width may affect the resulting geometry and a special attention should go to the assembly of different parts. Also in the slicing process there are some crucial parameters: the layer height, the infill percentage ("fullness" of the inside of a part) and pattern (structure and shape of the material inside of a part), the velocity (linked to bioink viscosity and resulting resolution) and the extrusion width [9].

This technology presents some advantages for the vascularization of tissues models: the possibility to print filaments of different diameters; the use of bioinks, whose composition can improve vascularization; the ability to control the spatial arrangement of the filaments to promote the formation of vascular networks, also with branched and complex geometries [12]. The filament diameter can be tuned varying the nozzle diameter, the printing pressure and speed, nevertheless it remains still restricted by the resolution limit.

1.4 Aim of the thesis

To date, however, 3D bioprinting has been used to achieve full-thickness vascularized tissues, but it has never been applied with the very purpose to obtain a vascular network for organoid perfusion. In the subtractive approach, indeed, a sacrificial network is bioprinted within a hydrogel scaffold that encapsulate tissue-specific cells which then grow surrounding the endothelialized vasculature up to the generation of the corresponding in vitro tissue with the already built-in vascular network, in the additive strategy the same result is instead reached by seeding tissue-specific cells onto the bioprinted vasculature (Figure 1.3) [4].

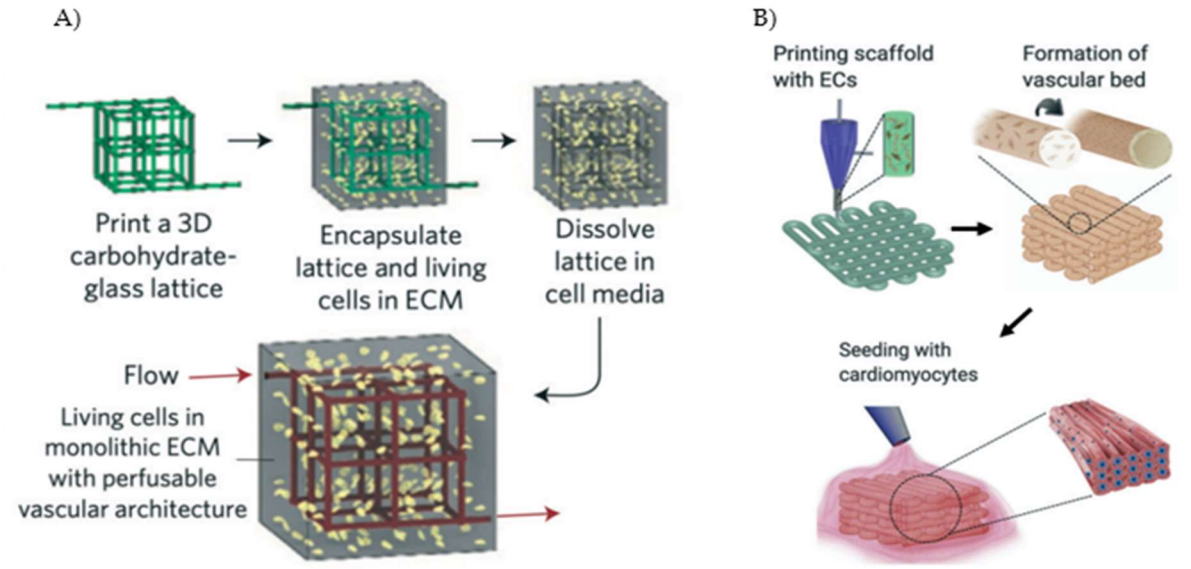

Figure 1.3 Subtractive (A) and additive (B) methods [4]

Hence, the present study aims to create a vascular network through 3D bioprinting to vascularize colon organoids. Such vascular network is bioprinted using a ECs-laden bioink, ECs then gradually migrate towards the periphery of the microfilaments generating a network of hollow endothelialized microfibers. Moreover, the grid is designed in order to host colon organoids: the network displays a central cavity with a suitable geometry replicating intestinal lumen with typical crypts and villi. Colon epithelial cells are then cultured in such a cavity to give rise to colon organoids.

This thesis work consisted in the optimization of the network bioprinting process. First of all, network geometry has been studied, then bioprinting parameters have been optimized and G-codes have been modified. After that biological experiments have been performed in order to evaluate endothelial cells distribution inside the network filaments and their survival along the culture. In the end colon epithelial cells have been seeded inside the vascular network.

2. Materials and Methods

2.1 3D Bioprinter and software

The printer and software used for the entire printing process, from 3D design to actual printing, are as follows:

1. CELLINK INKREDIBLE +: The INKREDIBLE+ 3D bioprinter (Figure 2.1) is a pneumatic-based extrusion bioprinter with dual printheads and UV LED curing system for bioprinting complex human tissue models and organs for tissue engineering research [19]. It is a cost-effective unit and it can be used as a standalone unit thanks to its LCD display and manual pressure regulators or it can be monitored through a computer with the accompanied software. After slicing, 3D CAD models are translated into coordinates and instructions for the INKREDIBLE+ to allow the bioprinter to move according to a defined path with a high XYZ resolution. The bioprinting process works through the extrusion of a bioink with or without cells in a bottom-up, layer-by-layer fashion until a 3D construct is built. INKREDIBLE + is compatible with standard petri dishes and multiwell plates and, once the construct has been bioprinted, it is crosslinked using the UV LED curing system (with wavelengths of 365 nm and 405 nm) or ionic solutions, depending on bioink's crosslinking requirements. Furthermore, the INKREDIBLE+ contains CELLINK's Clean Chamber Technology, that provides a sterile printing environment without the need for a biological hood. The two heated (room temperature to 130°C) printheads allow to print different cell types in the same structure and they are compatible with 3 mL cartridges, but also with aluminium cartridges, hence a wide range of bioinks can be used [20].

Figure 2.1 CELLINK INKREDIBLE + 3D bioprinter

2. SOLIDWORKS: SolidWorks is computer-aided design (CAD) software that uses the principle of parametric design to design very precise 3D objects [21]. It allows to save the 3D CAD model in different 3D file formats, including the STL format, which is the standard file type used by most 3D printing systems. The STL file is the triangulated representation of the 3D CAD model and the slicing software will be able to work with the SolidWorks model in STL format [22].
3. PRUSASLICER: PrusaSlic3r is a slicer software that can read STL files, it converts the 3D model into a series of thin layers and produces a G-code file containing instructions that tell the 3D printer exactly what actions to perform, where to move, what speed to use and more [17]. The software allows to choose the layers height, the infill percentage and pattern to fill the inside of the model, the printing velocities for the infill and perimeter, the nozzle diameter and the number of extruders. At last, the user can preview the G-Code before printing and, if everything looks alright, the G-code can be exported [23], [24]. Then it is submitted to post-processing through Spyder, which is an open-source cross-platform integrated development environment for scientific programming in the Python language [25], [26].

2.2 Cells and culture media

Cells and respective culture media used in the present study are as follows:

1. EAhy926: EA.hy926 is a hybridoma line derived from human endothelium and A549/8 cells [27]. They display stable endothelial characteristics and can be used for cardiovascular disease research [28]. Electron photomicrographs demonstrate cytoplasmic distribution of Weibel-Palade bodies and tissue-specific organelles, characteristics of differentiated endothelial cell functions such as angiogenesis, homeostasis/thrombosis, blood pressure and inflammation [29], [30]. EAhy926 growth conditions are 37°C, 95% air, 5% CO2 and complete DMEM as culture medium.

2. HUVEC GFP: HUVEC are normal primary human umbilical vein endothelial cells isolated from the vein of human umbilical cord and cryopreserved as primary cells to ensure the highest viability and plating efficiency [31]. They are a model system for studying endothelial cell function, with applications including hypoxia, inflammation, oxidative stress, response to infection and both normal and tumour-associated angiogenesis [32]. HUVEC growth conditions are 37°C, 95% air, 5% CO2 and C-22111 Endothelial Cell Growth Medium by Sigma-Aldrich as culture medium.

3. HEK-293 GFP: 293 [HEK-293] is a cell line exhibiting epithelial morphology that was isolated from the kidney of a human embryo. This cell line can be used in industrial biotechnology, toxicology research and drug development *in vitro* models. It has applications in efficacy testing and viruscide testing [8]. HEK293 GFP stable cells express transgenically GFP (Green Fluorescent Protein), so their proliferation and trafficking can be monitored by fluorescence imaging [33], [34]. HEK-293 GFP growth conditions are 37°C, 95% air, 5% CO2 and complete DMEM as culture medium.

4. H5V GFP: H5V is a murine endothelial cell line isolated from embryonal heart [35], [36]. H5V GFP cells express GFP, so when excited by blue light they emit green light and can be detected with fluorescence microscope. H5V GFP growth conditions are 37°C, 95% air, 5% CO2 and complete DMEM as culture medium.

5. CACO2: Caco-2 [Caco2] are human epithelial cells isolated from colon tissue derived from a 72-year-old white male with colorectal adenocarcinoma [37]. This cell line is primarily used as a model of the intestinal epithelial barrier and it has applications in cancer and toxicology research [38]. In culture Caco-2 cells spontaneously differentiate into a monolayer of cells that express characteristics of enterocytic differentiation [39]. Caco-2 growth conditions are 37°C, 95% air, 5% CO2 and complete DMEM as culture medium.

2.3 Hydrogels

Hydrogels used in the present study are as follows:

1. CELLINK FIBRIN GEL: CELLINK FIBRIN (Figure 2.2), based on CELLINK Bioink, contains nanofibrillated cellulose and these nanosized fibrils make the bioink semi-translucent allowing cell imaging and analysis. Additionally, this bioink includes fibrinogen that is converted into a fibrin network with thrombin-containing crosslinking solution after printing. This in situ fibrin protein network provides a physiologically relevant wound-healing environment that mimics blood clotting and supports vascularization [40]. Moreover, this bioink contains low levels of endotoxins that allow the creation of healthy and diseased tissue models with minimal interference with drugs during drug discovery and development research. CELLINK FIBRIN is available in 3 mL cartridges and it must be stored at 4-8°C [41].

Figure 2.2 CELLINK FIBRIN cartridge

1) CELLINK GELMA C: GelMA C (Figure 2.3) combines the advantages of bioactive GelMA with nanofibrillated cellulose and these nanosized fibrils make the bioink translucent allowing cell imaging and analysis [42]. This bioink is crosslinked after printing through photoinitiator activation (LAP at 0.25%) by exposure to UV and near-UV light. GelMA C offers smooth printability at ambient conditions and low extrusion pressures using a wide range of nozzle diameters, it is available in 3 mL cartridges and it must be stored at 4-8°C [43].

Figure 2.3 GelMA C cartridge

2) MATRIGEL: Matrigel is a solubilized basement membrane preparation extracted from the Engelbreth-Holm-Swarm (EHS) mouse sarcoma, a tumour rich in extracellular matrix proteins [44]. It has a heterogenous composition, its major components are laminin, collagen IV, nidogen, heparan sulphate proteoglycans and growth factors [45]. Matrigel promotes the differentiation of many different cell types and the outgrowth of differentiated cells. It is stored as a frozen solution at -20°C in a non-frost-free freezer, it should be thawed overnight in a 4°C refrigerator, it gels at 24–37°C in 30 min and the gelling is irreversible with cooling [46]–[48]. Cells are generally plated on top of the gelled material, but can also be mixed with the matrix prior to gelling. Cells on or in this matrix associate with each other usually in 3D and then form structures like those in the tissue of origin. Many cell lines and primary cells do not proliferate, but differentiate in presence of this matrix. Both the morphology and the genes expressed by cells indeed reflect a more differentiated phenotype, however the differentiation response depends on the cell type [49].

2.4 Microscopy

The microscope, the microscopy softwares and the fluorescence quantification procedure used in the present study are as follows:

1. MICROSCOPE: In the present study the Eclipse Ti2 Inverted Microscope has been used into 2 modalities: bright-field mode for cell passages and counting, but also for image visualization and acquisition through the designed software of the structures without cells or with non-GFP cells; fluorescence mode instead for the structures with GFP cells that emit

bright green light (lambda max = 509 nm) when excited with blue light (lambda max = 395 nm, minor peak at 470 nm).

2. NIS ELEMENT VIEWER: it is an integrated software imaging platform which provides complete microscope control, visualization, image capture, documentation, image analysis and data management [50]. It can acquire full bit depth multicolour images combining multiple fluorescence wavelengths and different illumination methods (differential interference contrast, phase contrast etc.) [51]. In the present study it has been used to acquire images both in bright-field and fluorescence.

3. IMAGEJ: ImageJ is a Java-based image processing program widely used in biological sciences [52]. It can display, edit, analyze, calibrate, process, save and print 8-bit, 16-bit and 32-bit images. It can read many image file format, including TIFF, PNG, GIF, JPEG, BMP, DICOM, and FITS, as well as raw formats. It can calculate area and pixel value statistics of user-defined selections and intensity-thresholded objects, it can measure distances and angles, it can also create density histograms and line profile plots. Moreover, it supports standard image processing functions, such as contrast manipulation, sharpening, smoothing, edge detection and median filtering. Additionally, density and grey scale calibration is available as well as spatial calibration to provide real world dimensional measurements in units such as millimetres. In the present study ImageJ has been used to quantify fluorescence intensity in the acquired images of GFP cells within the printed structures along the culture days.

4. FLUORESCENCE QUANTIFICATION: in order to quantify green fluorescence intensity in a 2D image (24 bit, TIF format in this case) using ImageJ, the first step is to split the RGB composite image (Figure 2.4 A) into separate channels (blue, green and red) and select the green one (Figure 2.4 B). Then it's important to tick the measurements required as data in the section "set measurements", such as area, mean grey value (sum of the grey values of all the pixels in the selection divided by the number of pixels), integrated density IntDen (sum of pixel values divided by the area), standard deviation and min & max grey value. Moreover, limit to threshold must be checked to use thresholding, in fact the threshold of the image must be adjusted to distinguish fluorescent cells from the background (Figure 2.4 C). To prevent the original image from being lost, creating a mask is crucial in order to have a binary image where only cells are selected (Figure 2.4 D). After processing the mask to smoothen the binary image or remove outliers and isolated pixels etc., a selection of the cells can be created (Figure 2.4 E), analysed and measured to get the values of the binary image. This selection has to be added on the ROI manager and then applied to the original image (Figure 2.4 F). Clicking on "measure" the ROI manager adds measurements to the results table, including IntDen which is the main value of interest, indeed it measures the fluorescence intensity of all the GFP expressing cells in the image. This value has to be measured for all the acquired images of a certain day in order to calculate the mean value and the standard deviation of that day. The same procedure has to be repeated for all the following days in order to have the trend of fluorescence intensity over time, that is an indicator of cells viability and proliferation, given that only alive cells express the GFP protein [53].

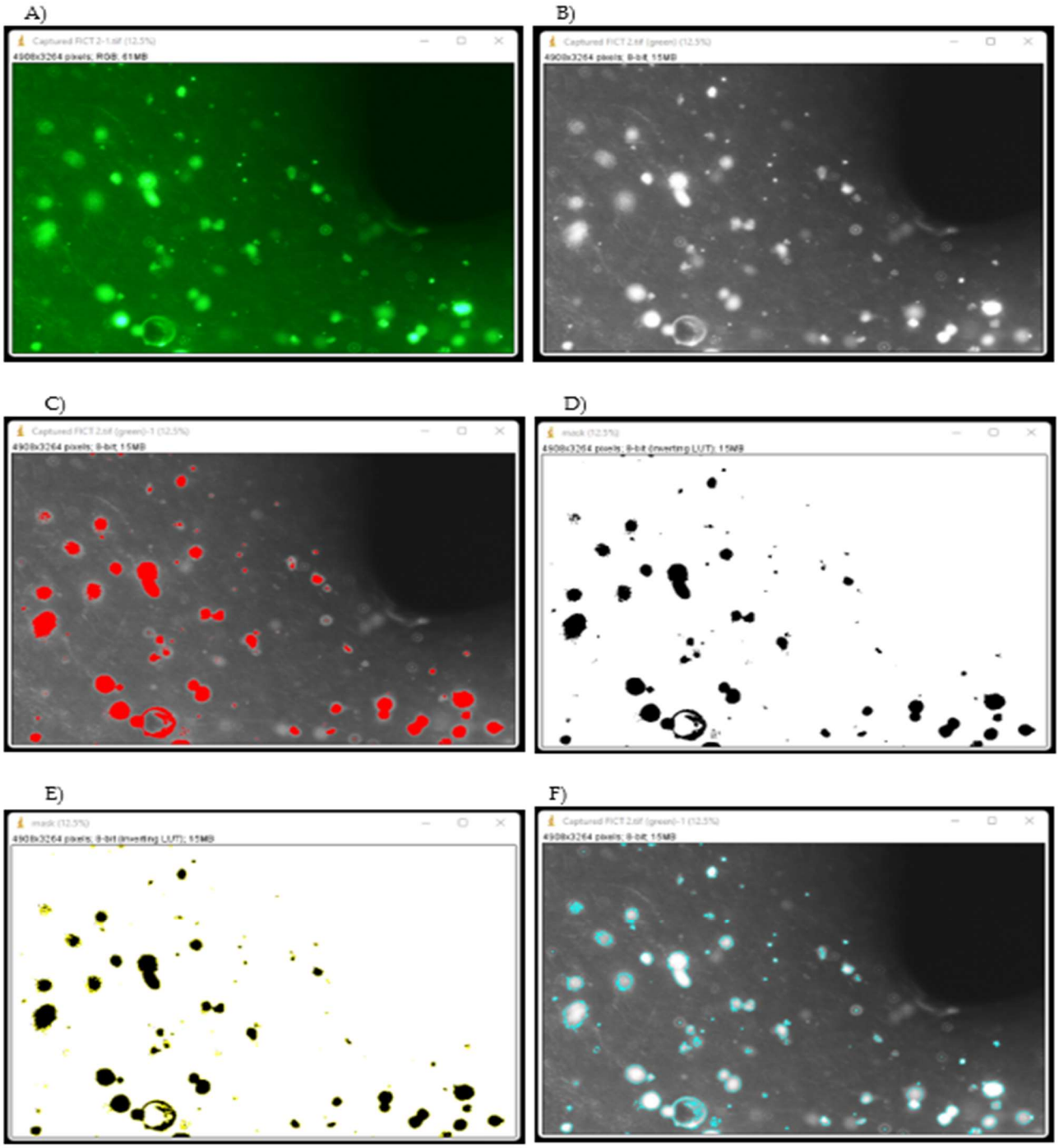

Figure 2.4 Fluorescence quantification steps

2.5 Bioprinting protocol

The following protocol is used for bioprinting both CELLINK FIBRIN and GelMA C with or without cells and must be performed in compliance with the rules for sterility maintenance.

This protocol can be carried out with a printhead at room temperature for CELLINK FIBRIN, while for GelMA C the printhead has to be pre-heated to 26°C, where room temperature is between 20-25°C. First of all the CELLINK FIBRIN cartridge has to be warmed up from the fridge

to room temperature under the biosafety cabinet, while GelMA C cartridge has to be heated for 15 min at 37°C in the incubator [54], [55].

Then the bioink (whether it is CELLINK FIBRIN or GelMA C) has to be mixed with cells 10:1 under the biosafety cabinet taking care not to introduce air bubbles and not to lose too much material during the different steps of whole procedure: the bioink has to be transferred from the cartridge to a 3 ml syringe using a luer lock adaptor, then also cell suspension has to be transferred to a 3 ml syringe using a microtip and lastly, they can be mixed together connecting the two syringes with a luer lock and mixing back and forth until homogeneity is reached (Figure 2.5) [54].

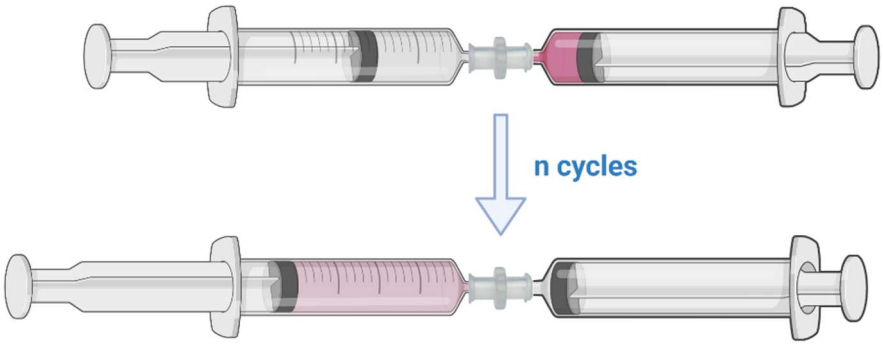

Figure 2.5 Schematic illustration of the mixing process between the bioink and cell suspension

To avoid incorporating too much air, syringe piston has to be pulled out and pushed back before usage to release the air inside. Additionally, another trick to avoid an air gap is to carefully pre-fill the luer lock adaptor with the bioink before attaching both the empty syringe and then the one with cell suspension [56]. After that the mixture has to be transferred back to the cartridge using a luer lock, taking care not to waste too much bioink. To recover the bioink left in the luer lock, the syringe can be detached, filled with air and reconnected to push the bioink towards the cartridge.

After being capped with the nozzle, the cartridge can be therefore mounted into the printhead. The recommended nozzle size is 22 G (0.41 mm), in fact a decrease in the nozzle diameter to achieve a thinner filament could increase the risk of bioink clogging, but could also cause cell suffering [54].

After the calibration of the bioprinter, eventually the structures can be printed and the pressure can be adjusted with the manual knobs to extrude more or less material and control filament diameter. It should not be waited too long between extrusions to prevent the bioink from drying in the nozzle causing it to clog, with the need to replace it with a new one. Moreover, even more attention should be paid when working with small volumes of bioink and cell suspension, introducing air becomes easier and some material could be lost, further reducing the final volume in the cartridge, with the risk that the bioprinter cannot succeed in extruding the bioink.

Furthermore, when GelMA C is used a few more precautions are necessary, especially because CELLINK INKREDIBLE + does not have a cooled print bed and, thus, the bioink may not perform as expected and resulting filament characteristics may be inconsistent. First of all, specific orange UV protected cartridges must be used to avoid crosslinking before printing, then, after cell mixing, the cartridge has to be left under the fumehood for 20 min to reach room

temperature (20-25°C) [55]. Moreover, the petri dishes or well plates have to be precooled a whole night in the fridge before printing, while they have to be placed 5 min in the fridge to thermally gel the structures after printing prior to photocrosslinking.

After that, the printed constructs can be crosslinked one after the other for 1 min using the 405 nm photocuring module at a distance of 5 cm. This module is in fact recommended compared to the 365 nm one, because an over exposure at this wavelength might damage cells [57]. Since culture medium is not present during this procedure, it should not last too long to avoid cell dehydration. Lastly, after crosslinking, the desired medium can be added to cover the constructs, that can be thus cultured in standard conditions. Following all these measures is crucial to achieve a suitable bioink printability, to prevent the printed structures from dissolving and to avoid cell suffering.

3. Results and discussion

3.1 Preliminary studies about structures geometry

The initial idea of the present work was to build a vascular network by printing a 3D lattice made up of crossed filaments and provided with a central cavity for organoids growth. In order to create this grid, a parallelepiped with a square base had to be designed on SolidWorks and then sliced with a low infill density in order to get a network of filaments instead of a full structure (Figure 3.1).

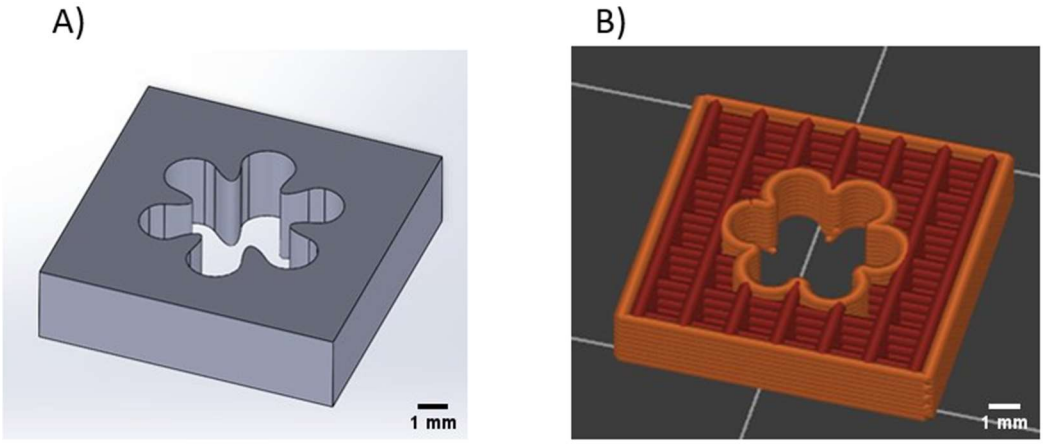

Figure 3.1 Construct designed with SolidWorks (A) and then sliced with PrusaSlic3r (B)

Initial printings were performed by printing a commonly used demonstration ink for extrusion-based 3D printing, which is the Nivea cream for body care [58]. Indeed, this lotion is one of the best accessible printable materials, it is cheap, has a constant quality and composition, is a soft colloidal ink and shows very good printing fidelity [59]. However, as with most hydrogels, her viscosity can be affected by different variables, among which the temperature, so in the present study the printing pressure could not be strictly defined, but it had to be adjusted according to the slight variations of the room temperature of the day experiment in order to get a sufficiently thin and continuous filament, always bearing in mind that excessive pressure can result in cell damage. Nevertheless, pressure ranged between 12 and 30 KPa.

These first studies were carried out without using cells and thus, since there was no need of maintaining sterility, the printer airflow could be set to zero and the petri dishes used were not sterile.

Another issue that was faced was the choice of the nozzle size to achieve a sufficiently thin filament without giving rise to excessively high shear stress that could harm cells. Indeed, the shear stress on the wall of the nozzle tip may damage the living cells and it should be controlled within 5 kPa to have more than 96% cell survival [60], [61]. A good compromise is the 0.41 mm-diameter conical nozzle that ensures a good resolution and cell viability. It was therefore selected in the present study, as it was also suggested by the bioprinting protocol.

Preliminary printing experiments were performed to determine the suitable infill pattern of the grid, infill percentage, structure height and printing velocity. The first printed constructs were parallelepipeds with a square base 1 cm x 1 cm of various heights, namely 0.8, 1.2, 1.6 and 2 mm, corresponding respectively to 2, 3, 4 and 5 layers (layer height=0.4 mm). They were printed with different combinations of infill patterns and densities: rectilinear (15, 30, 50%), gyroid (30, 50%) and honeycomb 3D (25, 50%) infill (Figure 3.2).

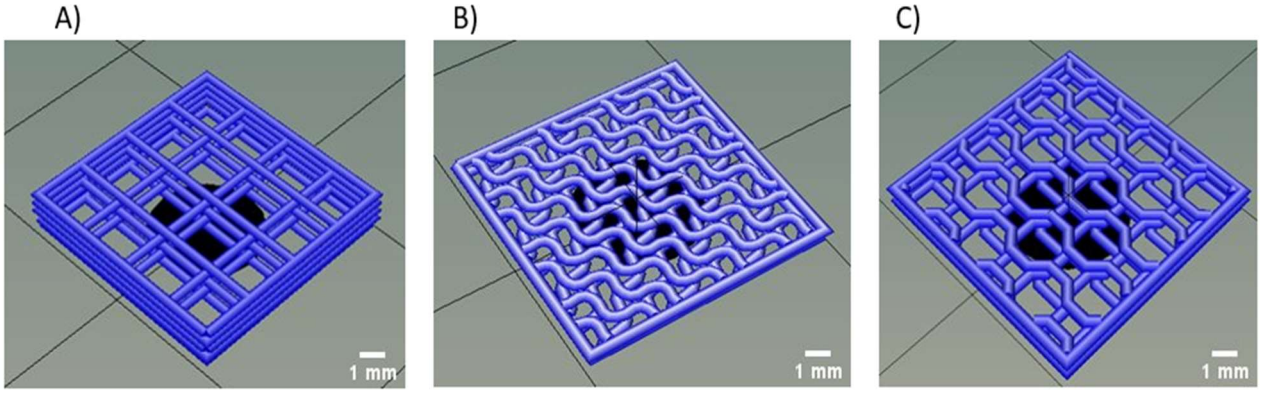

Figure 3.2 Constructs with different infill percentage, pattern and height: A) 15% rectilinear infill h=2 mm, B) 50% gyroid infill h=0.8 mm and C) 25% honeycomb 3D infill h=1.2 mm

Best results were obtained with the rectilinear pattern, which creates a rectilinear grid by printing one layer in one direction, the next layer rotated by 90° and so on. This pattern was in fact the best reproduced by the printer in terms of shape fidelity and retention, filament uniformity, non-merger of the parallel fibres, but also of the fibres overlapped layer-by-layer. The honeycomb 3D pattern was, instead, the worse one, mainly because of fibres merging and low print fidelity. As for the infill density, the percentages up to 30 gave better results in terms of split fibres, while 50% infill led to merging fibres and reduced shape retention.

Moreover, initial printing speed was set to 10 mm/s both for perimeter and infill, giving good results in terms of standing structures up to 3 layers, but an interrupted filament (especially in the inner part of the construct) and/or collapsing structures for taller geometries. Velocity was thus reduced to 6 mm/s obtaining better results also for taller geometries, but with a thicker filament. At the end of these first experiments final parameters were as follows: 15% rectilinear infill patter, printing rate of 10 mm/s for constructs up to 3 layers, while a printing rate of 6 mm/s for 4- and 5-layers constructs.

Once selected the infill and the speed, the second aspect to be defined was the geometry of the internal hole of the grid, intended to host colon organoids. Two kinds of geometries were studied, on the one hand a simple 3x3 mm^2-square hole and on the other hand a flower-like hole with a 5 mm-external diameter that aimed to resemble the colon crypts and villi geometry, as the external part of the "petals" represented the crypts and their inner part, protruding in the hole lumen, the villi. These different hole geometries were tested into two kinds of 2 mm-high (5 layers) grids: grids

with a 9.7x9.7 mm^2 -base and a single central hole and grids with a 15x15 mm^2 -base and 4 holes (Figure 3.3), with the purpose of culturing 4 organoids simultaneously. The constructs were printed with low (6 mm/s) printing velocity and 15% rectilinear infill.

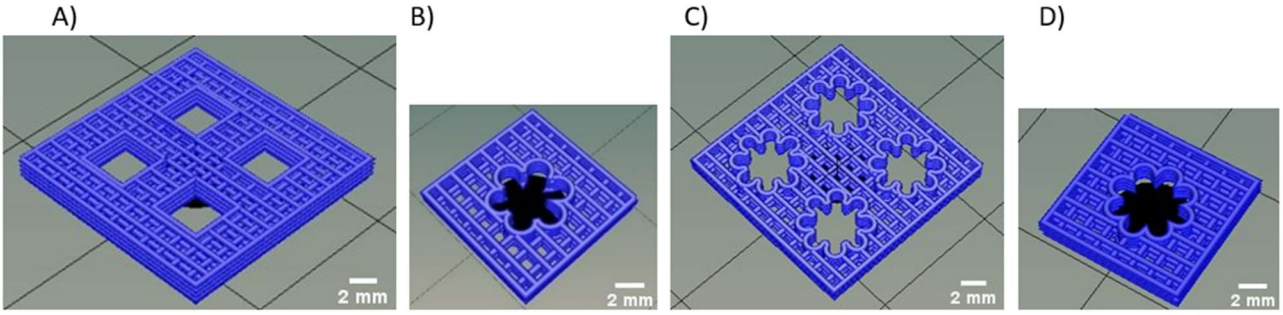

Figure 3.3 Different geometries of the holes: A) 3x3 mm^2 square, B) 40°-6 petals flower, C) 22.5°-8 petals flower and D) 27°-8 petals flower

To design the "flower" on SolidWorks a circle was divided into circular sectors by a certain number of diameters (twice the number of desired petals), then designing arcs and erasing some lines, half of these sectors were transformed into petals and the other half into spaces between two consecutive petals (Figure 3.4). The circular sectors could be all of the same size or of alternating sizes, giving rise to petals bigger than the spaces between two petals. The different geometries tested were as follows: flowers with a 3 mm-inner diameter and 4 petals of 45°, flowers with a 3 mm-inner diameter and 6 petals of 30° or 40°, flowers with 8 petals of 22.5° and a 3/3.5/4 mm-inner diameter and flowers with 8 petals of 27° and a 3.5 mm-inner diameter.

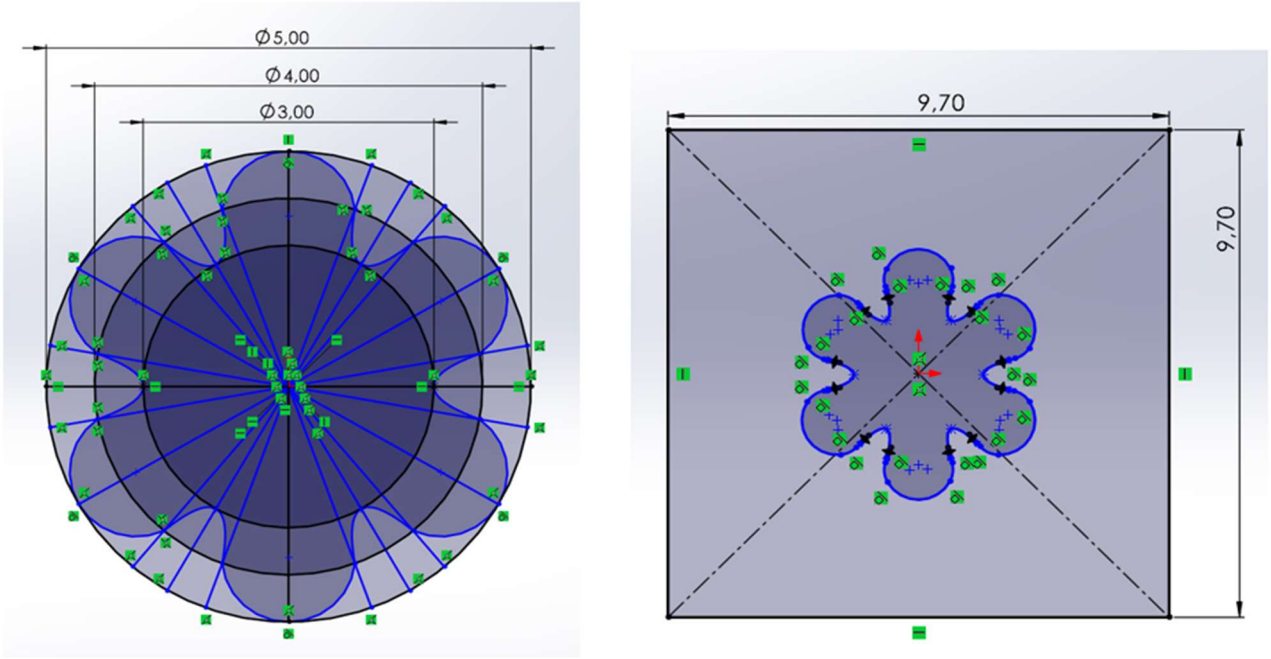

Figure 3.4 Process to design the flower-like hole

While on the one hand the square holes were optimally printed, but didn't mimic the colon anatomy, on the other hand reproducing faithfully the flower-like design with a high resolution was more challenging. In the latter case best results were reached with the 40°-6 petals flowers.

The slow speed required to print these 5-layers structures gave rise to a filament that might not have the desired thinness, but increasing the velocity up to 8 mm/s for perimeter (keeping 6 mm/s for infill) the constructs collapsed (Figure 3.5). Therefore, the resulting parameters of these experiments were square holes and 40°-6 petals flower-like holes, with a slow printing rate of 6 mm/s both for perimeter and infill.

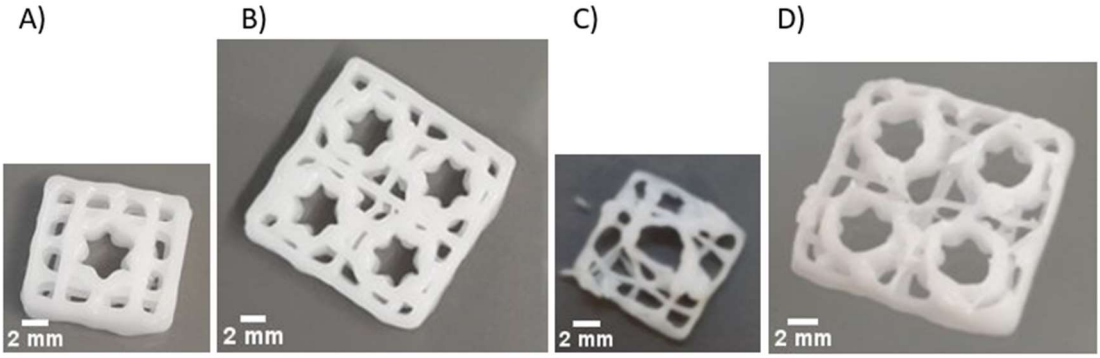

Figure 3.5 Constructs printed with a slow speed (A and B) and with a higher speed (C and D)

At the same time there was the need to print monolayer structures for cell imaging. The same grids with one or four holes of different geometries were tested, but their height was 0.4 mm (1 layer) instead of 2 mm. Since the superimposed layers collapse issue was not present, printing speed could be set to 8 mm/s for perimeter and 6 mm/s for infill, allowing to obtain a thinner filament. Moreover, the 15% rectilinear pattern was replaced by the grid pattern with 30% infill to get the same sized gaps in the final lattice. Unlike in the rectilinear pattern, the filament is indeed printed in both directions (rotated by 90°) in each layer. In this case best results were achieved with 3x3 mm^2 square holes and 6 petals flower-like holes of 40° for the single hole case, while of 30° for the four holes case (Figure 3.6).

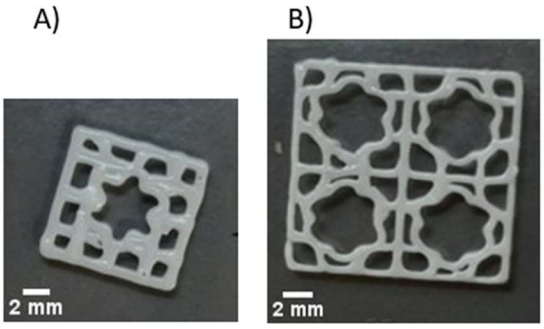

Figure 3.6 Monolayer structures with single central 40°-6 petals flower-like hole (A) and with four 30°-6 petals flower-like holes (B)

These preliminary studies led therefore to the ultimate definition of the geometries of the grids to be printed:

- 1 layer (0.4 mm):
  - 9.7x9.7 mm^2 grid with single central 40°-6 petals flower-like hole
  - 15x15 mm^2 grid with four 30°-6 petals flower-like holes
  - High velocity (8mm/s for perimeter and 6mm/s for infill)
  - 30% grid infill

- 5 layers (2 mm):
  - 9.7x9.7 mm^2 grid with single central 40°-6 petals flower-like hole
  - 15x15 mm^2 grid with four 40°-6 petals flower-like holes
  - Slow velocity (6mm/s both for perimeter and infill)
  - 15% rectilinear infill

Once established the geometry of the constructs, the following step was the definition of the process to obtain and culture the vascular network as well as colon organoids. Three different approaches were considered. The first one consists in the simple bioprinting of the endothelial cells-containing lattice, its culture up to the capillaries formation, the subsequent positioning of colon epithelial cells-laden Matrigel droplets inside the grid hollows and their culture up to the self-assembly into colon organoids. The second strategy is, instead, a 2-step bioprinting: first the vascular network is bioprinted and cultured, then colon epithelial cells are bioprinted inside the lattice hollows and cultured up to colon organoids formation. Last procedure is a dual printheads bioprinting that allows the simultaneous bioprinting of endothelial cells with one extruder and of colon epithelial cells with the other, all followed by vascular network and organoid culture.

3.2 2-Step printing

The second strategy, as well as the third one, required the definition of the geometry of the structures to be printed inside the holes of the different grids.

In order to study them, printing experiments were performed using Nivea cream both for the grid and for the internal structure. The external grid was printed first, then the petri dish was removed from the print bed and right after repositioned to mimic the procedure that would be performed with cells, at the end the internal structure was printed inside the grid hollow.

Concerning the grids, the four different kinds defined before were printed, while for the internal structures both flower-like and circular structures of different sizes were tested. We can distinguish four cases according to the external grid (Table 3.1):

Case N°	Type of external grid	External diameter of the inner flower-like structure (mm)	Diameter of the inner circular structure (mm)
1	monolayer grid with single hole	1.8, 2.2, 2.4	1.2, 1.4, 1.6, 2, 2.2, 2.4
2	monolayer grid with four holes	1.8, 2.2, 2.4	1.2, 1.4, 1.6, 2.4, 2.5, 2.6
3	5 layers-grid with single hole	1.8, 2.2	1.2, 1.4, 1.6, 2
4	5 layers-grid with four holes	1.8, 2.2	1.2, 1.4, 1.6, 2, 2.2

Table 3.1 Dimensions of the internal structures

Just like their respective grids, monolayer constructs were printed with a high speed (8 mm/s for perimeter and 6 mm/s for infill) to get a higher resolution, while the 5 layers constructs with a slow speed (6 mm/s both for perimeter and infill) to prevent collapse. An 80% rectilinear infill was chosen for all the internal structures, so that they could become a "full" environment enabling colon cells communication and migration and thus their self-organization in colon organoids.

Circular structures gave better results in all the four cases, respectively with a diameter of 2.2, 2.5, 2 and 2 mm (Figure 3.7). As for the other circular structures, their diameter was too big risking to overlap and damage the grid, or too small that the internal structure was too far from the grid preventing the two constructs from interfacing each other and, thus, hampering the possibility to vascularize organoids. Flower-like structures were, instead, dismissed mostly because they actually did not have such an accurate shape once printed.

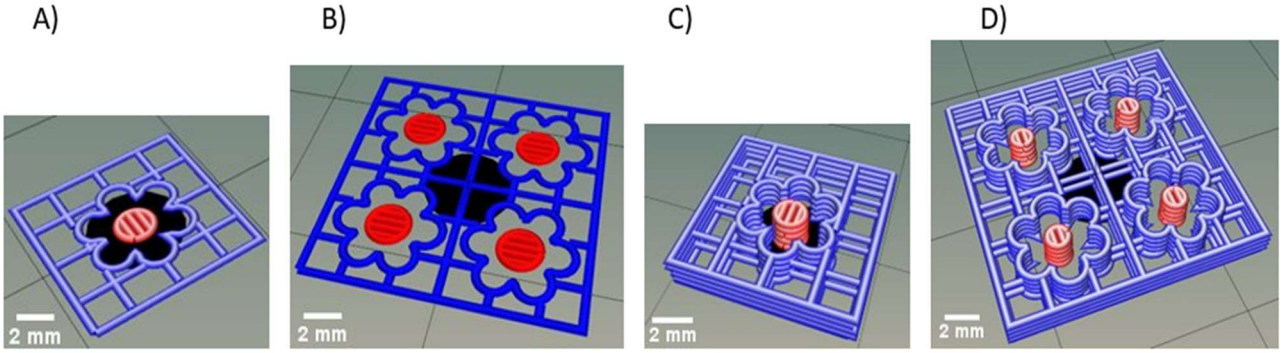

Figure 3.7 Final internal structures with a diameter of 2.2 (A), 2.5 (B), 2 (C) and 2 mm (D)

Although PrusaSlic3r (together with the Spyder postprocessing) generates functional G-codes, sometimes they are not perfect and have to be corrected and adapted to the specific case. This is one of those cases, mostly because the structures were printed inside a pre-existent construct instead of an empty petri dish. In fact, unfortunately, all these cases reported some issues related to printhead movements during the printing process that led to grid damage and filament displacement (Figure 3.8). In cases 1) and 3) this was due to the fact that the printhead went down touching the grid at the hole perimeter level and only then moved to the centre of the hole to print the internal structure dragging some material and thus ruining the grid. In case 2) in addition to this, grid damaging resulted also from the printhead movements with no lifting between the four different circular structures.

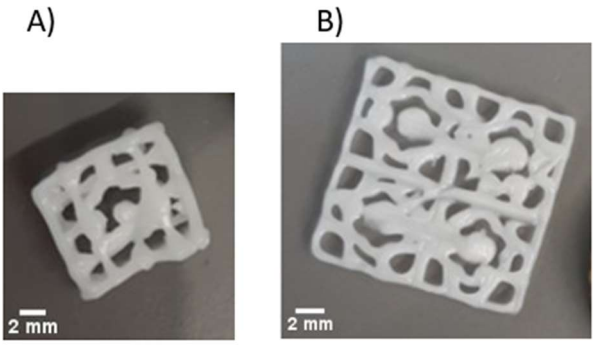

Figure 3.8 Structures damaged by printhead movements

A precisely centred printhead descent was necessary to solve the first problem, while in the second case also printhead raising and lowering between the four holes was essential. G-codes were modified to achieve these results. As for the first one, the printhead was moved along xy first and then along z directly to the hole centre, while for the second one, whenever a structure was printed, the printhead was lifted along z, then moved along xy towards the right position above the centre of the next hole, and finally it was lowered along z to print the next structure.

Concerning case 4), there were the same problems as case 2) that were solved in the same way, but there was also another hurdle to overcome. Indeed, according to the G-code generated by the slicer (and postprocessed), instead of printing every single cylinder from layer 1 to 5 and only then moving to the next one, the 3D printer printed the first layer of all the four structures and then moved to the second layer and so on, destroying the grid at each movement from a cylinder to another. The G-code was therefore modified so that the printhead went down right in the hole centre printing all the 5 layers of a cylinder, then it was lifted, moved towards the next cylinder and lowered into the next hole centre to print the whole next cylinder and so on.

Thanks to all these G-code modifications, all the hurdles of the 2-step printing could be overcome (Figure 3.9).

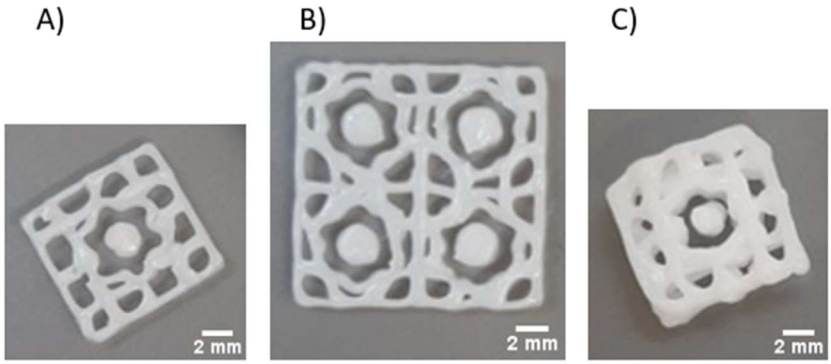

Figure 3.9 Structures correctly printed with no damage after G-codes modifications

3.3 Dual printheads printing

The third approach planned to print the same already optimized external and internal structures as the previous one, with the same printing rate and the same infill pattern and density, using the first printhead to print the grid and the second one for the internal circular structures. Exactly as before, the experiments were performed loading the 2 cartridges with Nivea cream to evaluate the proper functioning of the printing process.

To understand the issue, one must consider that, in dual extrusion printing, in every single layer a printhead-switch occurs. Care must be taken to prevent this switch, that happens lifting the active printhead and lowering the other, from ruining the already printed constructs. Moreover, all the previous problems were still present, such as the non-centred printhead descent and the movements between the four holes with no printhead lifting.

In case 1) the G-code was modified at the extruder switch so that the second printhead could be lifted and then lowered directly into the hole centre without touching the grid. The same for case 2) and additionally the printhead was lifted, shifted and lowered moving from a hole to the other preventing grid damage. As for case 3), the G-code was modified at each extruder switch so that the printhead lifted and lowered right in the print starting point without destroying the already printed structures. Finally in case 4) in addition to the changes made for case 3), the printhead was lifted and lowered passing among the four different cylinders, also during the layer shift.

This way all the G-codes were optimized so that the desired structures could be correctly printed (Figure 3.10).

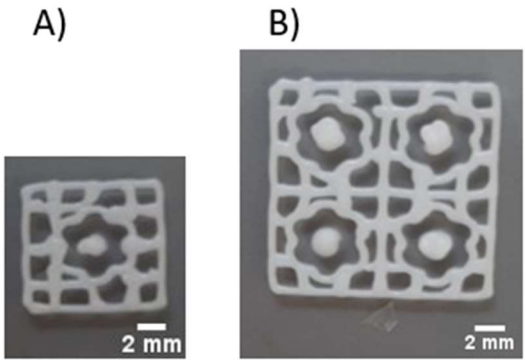

Figure 3.10 Structures correctly printed with no damage after G-codes modifications

3.4 Printing in 6-wells plates

Furthermore, to save time between subsequent printings and have a better chance to optimize the printing pressure of a certain construct to be printed, it was thought to simultaneously print several structures to analyse and grow many cultures under identical conditions. Thus, the structures were printed no longer in a petri dish, but in a 6-wells plate (Figure 3.11). To do so, the G-code of the desired structure was repeated 6 times, with the addition of the printhead rise, shift and descent between the wells. Moreover, there was also the need to calibrate the 3D printer so that it could have the centre of the bottom left well set as the new print starting point.

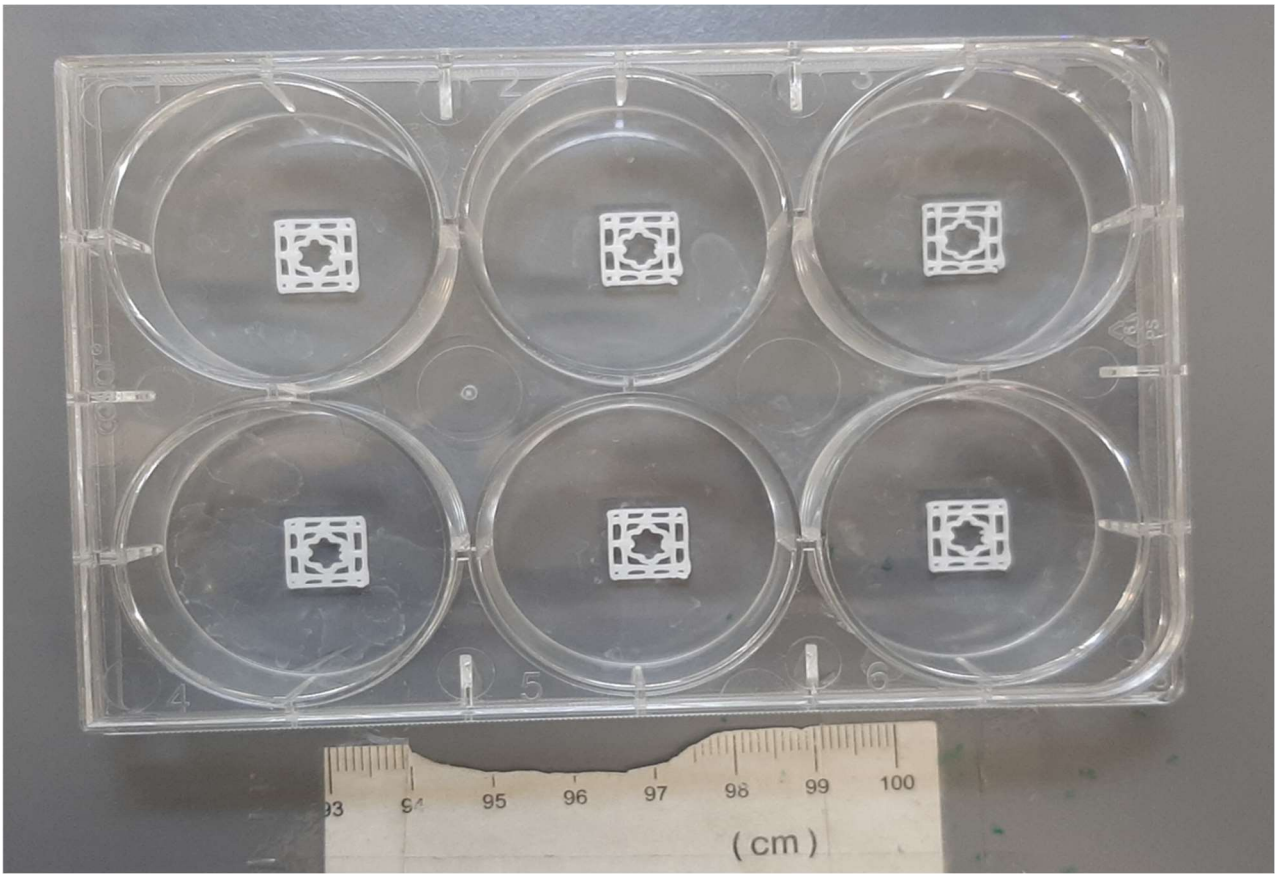

Figure 3.11 Printing of the same structure in a 6-wells plate

It must be remembered that, at the beginning of every printing process, the pressure must be calibrated to get a continuous filament and this requires the material to flow for a while until the appropriate pressure is found, dirtying though the culture support. When the construct is printed in a petri dish, the petri dish can be substituted with a new sterile one after pressure adjustment, maintaining thus sterility. In this case, instead, to avoid discarding a whole 6-wells plate, the G-code was further modified to print only 5 structures, leaving a free well for pressure regulation. This was simply made by deleting the last single structure-G-code repetition.

3.5 Bioink printed structures

Once defined all the geometries to be printed and verified the proper functioning of the different G-codes, the following step was to print the constructs using the desired bioink with no cells rather than Nivea cream, to assure that the same results in terms of printability and shape fidelity could be achieved also with the bioink.

CELLINK FIBRIN was the first bioink used, that was chosen for its capability to support vascularization [62]. The printed structures were the 9.7x9.7 mm^2-grid with single central 40°-6 petals flower-like hole and the 15x15 mm^2-grid with four 30°-6 petals flower-like holes, both 0.4 mm-high (1 layer) with a 30% grid infill and a high printing speed (8 mm/s for perimeter and 6 mm/s for infill). Pressure optimization (P around 25-27 KPa) allowed to achieve the desired outcomes (Figure 3.12).

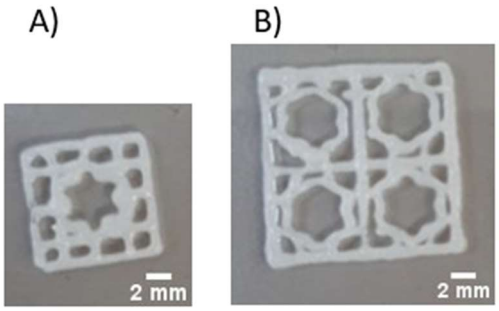

Figure 3.12 Monolayer structures printed using the CELLINK FIBRIN bioink: the 9.7x9.7 mm^2-grid with single central hole (A) and the 15x15 mm^2-grid with four holes (B)

Once verified this bioink was suitable for the bioprinting process, it was mixed 10:1 with EAHY cells (according to the bioprinting protocol) to print the 9.7x9.7 mm^2-grid 0.4 mm-high (1 layer) with single central 40°-6 petals flower-like hole with the same infill and printing rate as before.

Since cells were present, the 3D printer laminar airflow was turned on, the culture supports used were sterile and all the procedures were performed with the purpose of maintaining sterility.

Once optimized the printing pressure (P around 22-24 KPa), the construct could be correctly printed, but the CELLINK FIBRIN turned out to be too opaque for the cells to be clearly seen in bright-field microscopy (Figure 3.13).

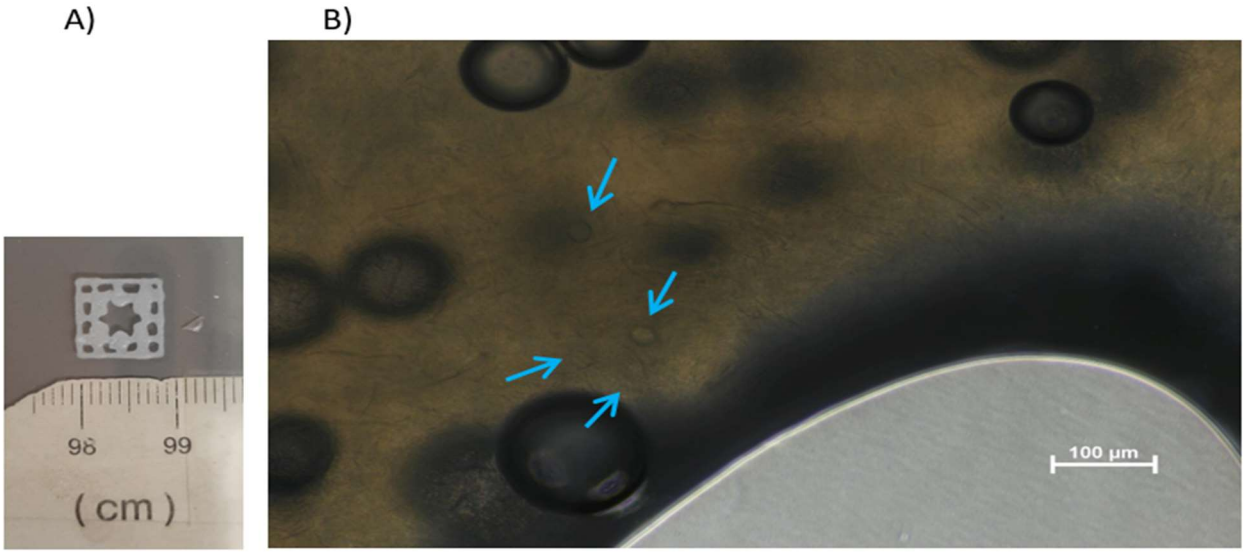

Figure 3.13 The opaque printed grid (A) and a filament of the grid seen in bright-field microscopy (B) with a few visible cells pointed by arrows

Three strategies were therefore adopted to overcome this hurdle: first of all, the structure height was reduced from 0.4 mm to 0.1 mm (through the modification of the structure height, but also of the layer height in PrusaSlic3r) so that cells could be better identified in a thinner layer (Figure 3.14); then the bioink was substituted with a translucent one, CELLINK GelMA C, to allow a better microscopic cells view; and last, GFP cells were used so that they could be detected with fluorescence microscopy.

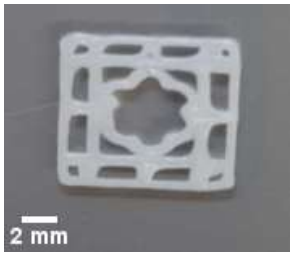

Figure 3.14 Grid with a height reduced to 0.1 mm

With the only purpose of checking if cells could be actually seen inside the new bioink, a first experiment was performed mixing GelMA C with EAHY cells (non GFP) and bioprinting the same grid as before, but 0.1 mm-high, with the printhead temperature set to 26°C, as required by the GelMA C bioprinting protocol. As hoped, this bioink turned out to be effectively transparent allowing cell imaging.

Once established the correct bioink to be used, another experiment was performed mixing GelMA C and HUVECs GFP 10:1 with a cellular density of $1.12*10^6$ cells/ml (cells number= $1.23*10^6$ cells).

5 grids (the same as the previous experiments) were printed in a 6-wells plate with an initial printing pressure of 9 KPa, that was gradually lowered to 6 KPa during the printing process to obtain a thinner filament. Then, after the 5 min required in the fridge, the grids were crosslinked using the 405 nm photocuring module for 1 min, macroscopic and fluorescent images were acquired (day 0),

structures were covered with the HUVECs-specific warm culture medium (4 ml per well) and the 6-wells plate was placed in the incubator.

Images were acquired for about 20 days (day 1, 4, 6, 11, 16, 19) (Figure 3.15) and during these culture days fluoresce microscopy allowed to see an initial slow increase in cells number and fluorescence intensity which then became higher, suggesting that cells were growing, followed by a stabilization phase during which the number of cells and fluorescence intensity remained almost unchanged and, in the end, cells started decreasing in number as well as fluorescence intensity, symptom that they were dying.

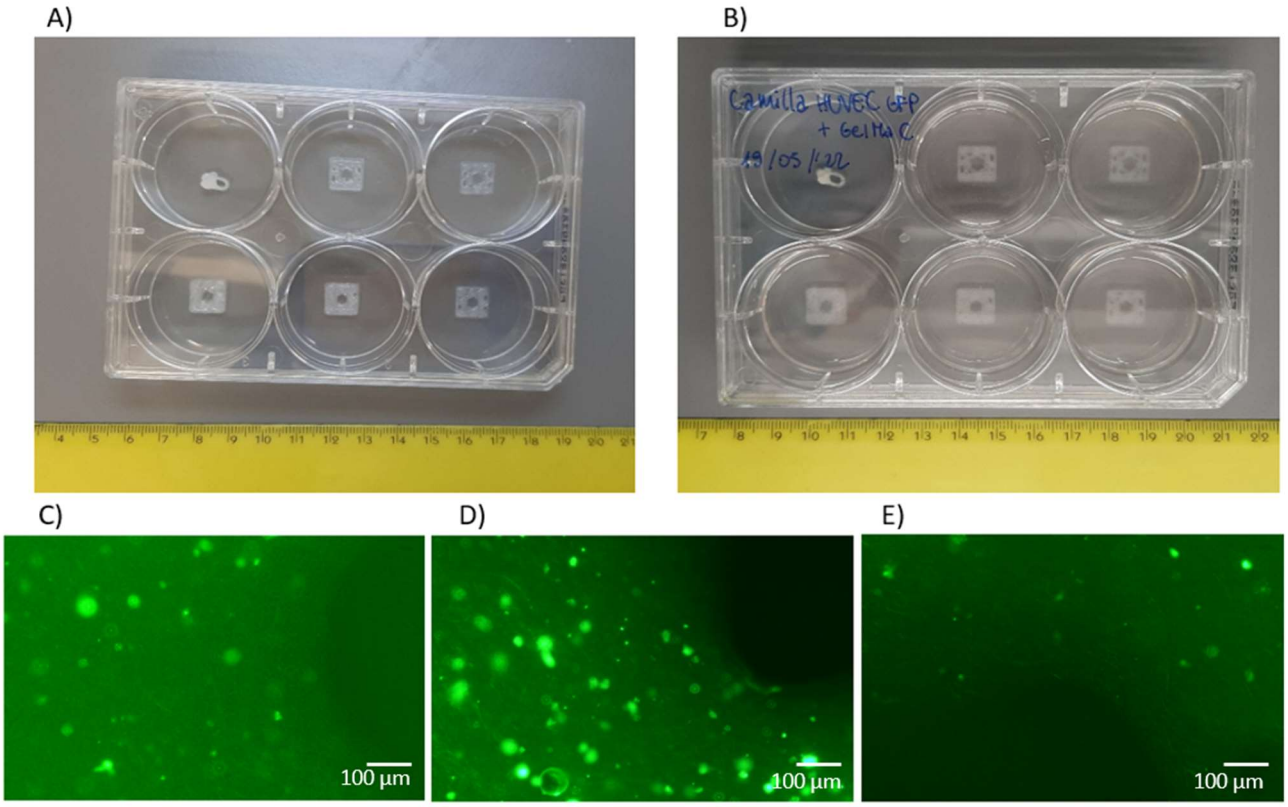

Figure 3.15 Macroscopic images of the printed grids on day 0 (A) and day 19 (B) and fluorescence microscopy images of the grid filaments on day 0 (C), day 6 (D) and day 19 (E)

During these 20 days of culture the bioink structures did not dissolve, shape and consistency were retained, demonstrating that the bioink was correctly crosslinked: 1-minute photocuring was a good compromise between hydrogel polymerization and cell survival. Moreover, no contamination occurred, proof that all the proceedings were performed in sterility conditions.

Fluorescence quantification results confirmed what expected (Figure 3.16).

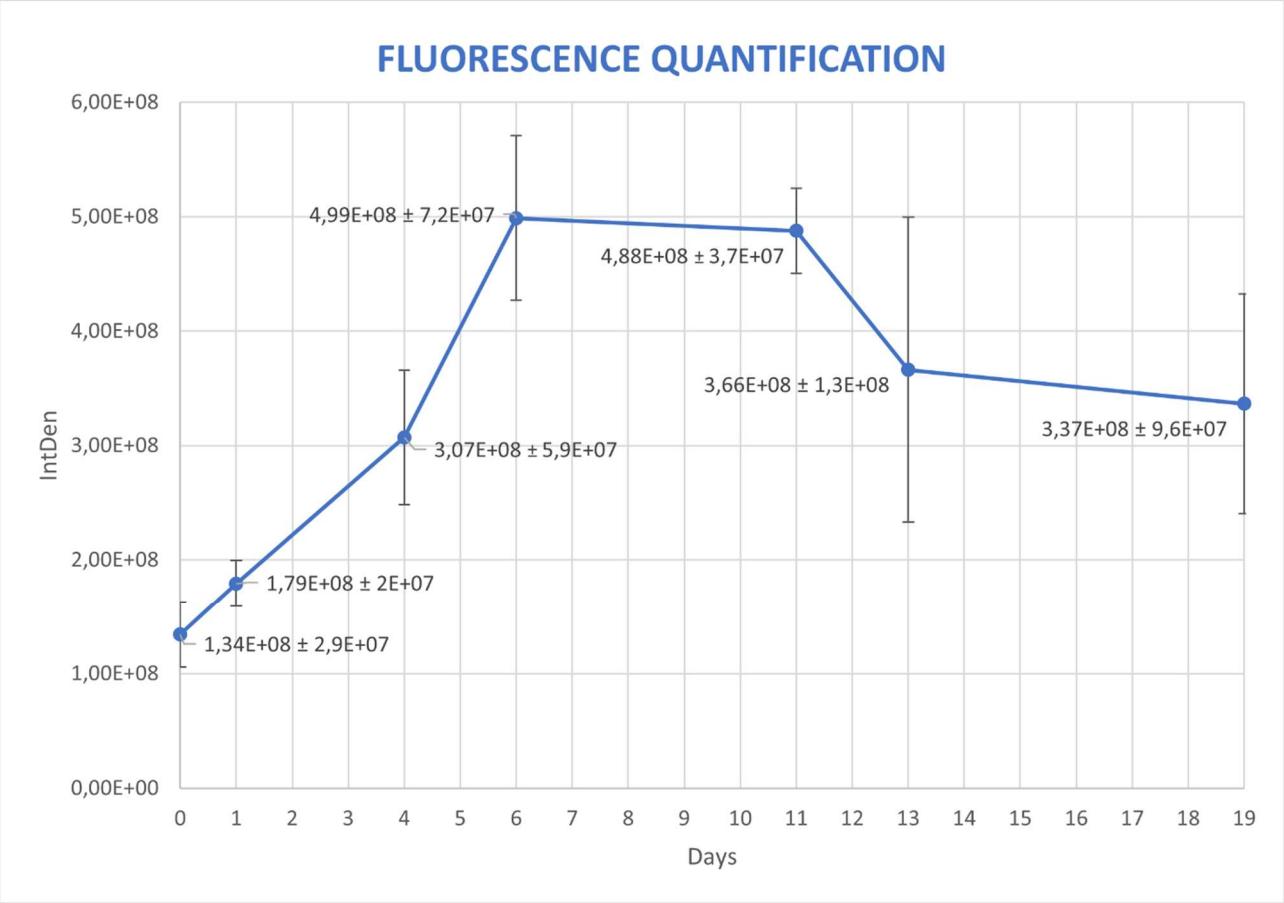

Figure 3.16 Graph of the fluorescence intensity (IntDen) along the culture days (from day 0 to 19)

The curve trend shows indeed an initial slow increment in fluorescence intensity, which later becomes faster, then a sort of plateau is present, followed by a rapid decrement that eventually becomes slower.

In order to validate the previous procedure, evaluate again cell distribution and vitality, another experiment was performed replicating the same conditions, but mixing GelMA C with HEKs GFP with the same cell density.

The same 5 grids were printed in a 6-wells plate, however in this case the bioink was initially too liquid that it came out from the nozzle in droplets and couldn't be extruded as a filament. This was probably caused by room temperature that was higher (29°C) than that of 20-25°C recommended by CELLINK protocol. Hence GelMA C bioink, after being incubated at 37°C for 15 min, mixed with cell suspension (with a 37°C-warmed medium), placed 20 min under the biosafety cabinet to reach room temperature and lastly inserted in the 26°C-preheated printhead (everything as required by the protocol), perhaps did not reach 26°C when printed, but had a higher temperature.

The cartridge was therefore put 5 min in the fridge to cool the bioink, which was then printed with a pressure of 8 KPa even though the gel was still quite liquid. After 5 min in the fridge, the constructs were crosslinked for 1 min, macroscopic and fluorescent images were acquired (day 0), warm culture medium was added (3 ml per well) and the 6-wells plate was placed in the incubator.

Images were captured for about 10 days (day 1, 2, 6, 9) (Figure 3.17) and during this culture period the bioink constructs gradually dissolved in the medium, as it could be seen with the naked eye, but

also proved by the decrease in the medium quantity required to cover the structures. Although the attempts to cool the bioink and the photocrosslinking, viscosity was not high enough for shape retention and this caused, as it could be seen at the microscope, some cells escaped from the bioink structures and their distribution over the well surface. Hower at least no contamination took place during the culture period, so sterility conditions were fulfilled also in this experiment.

Since the beginning fluorescence microscopy showed a poor number of cells inside the filaments and a low fluorescence intensity, which then slightly increased and eventually stabilized. A subsequent decrease, indicative of cell death, could not be detected since the structures dissolved earlier, thus preventing from image capture for longer periods.

The main issue of this low cell viability was not related to the bioprinting process and culture, but to room temperature that did not enable to print a bioink capable of providing cells with a suitable environment in which to be retained and proliferate.

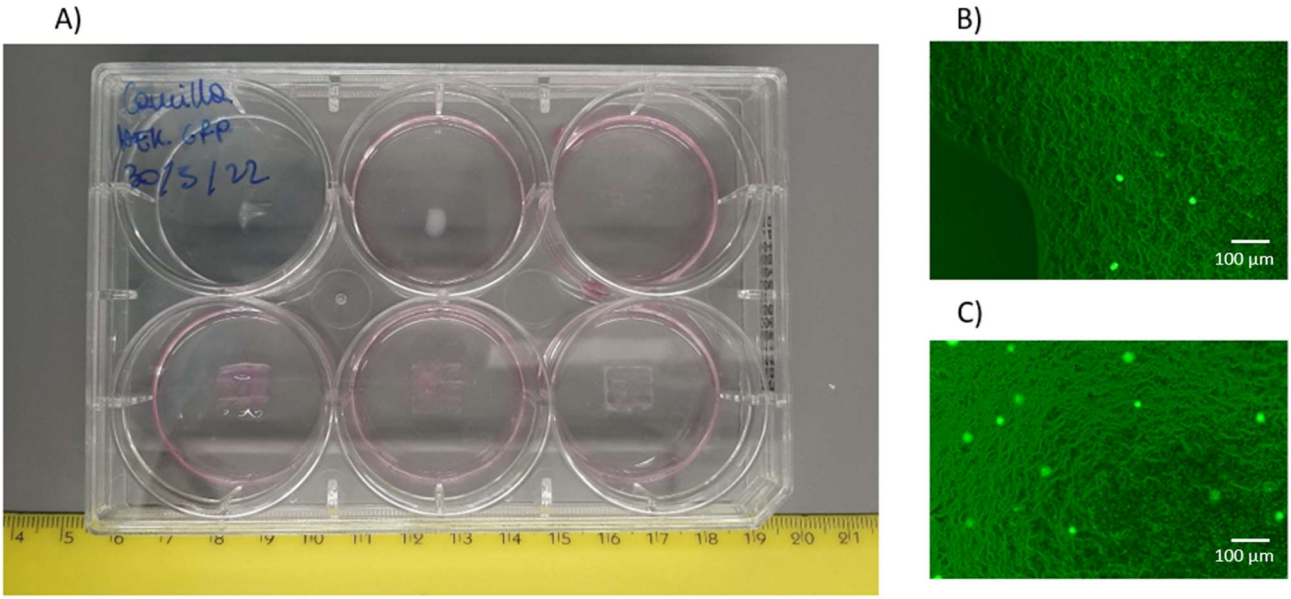

Figure 3.17 Macroscopic images of the printed grids on day 2 (A) and fluorescence microscopy images of the grid filaments on day 0 (B) and day 2 (C)

Visual assessment was further supported by the fluorescence quantification analysis (Figure 3.18).

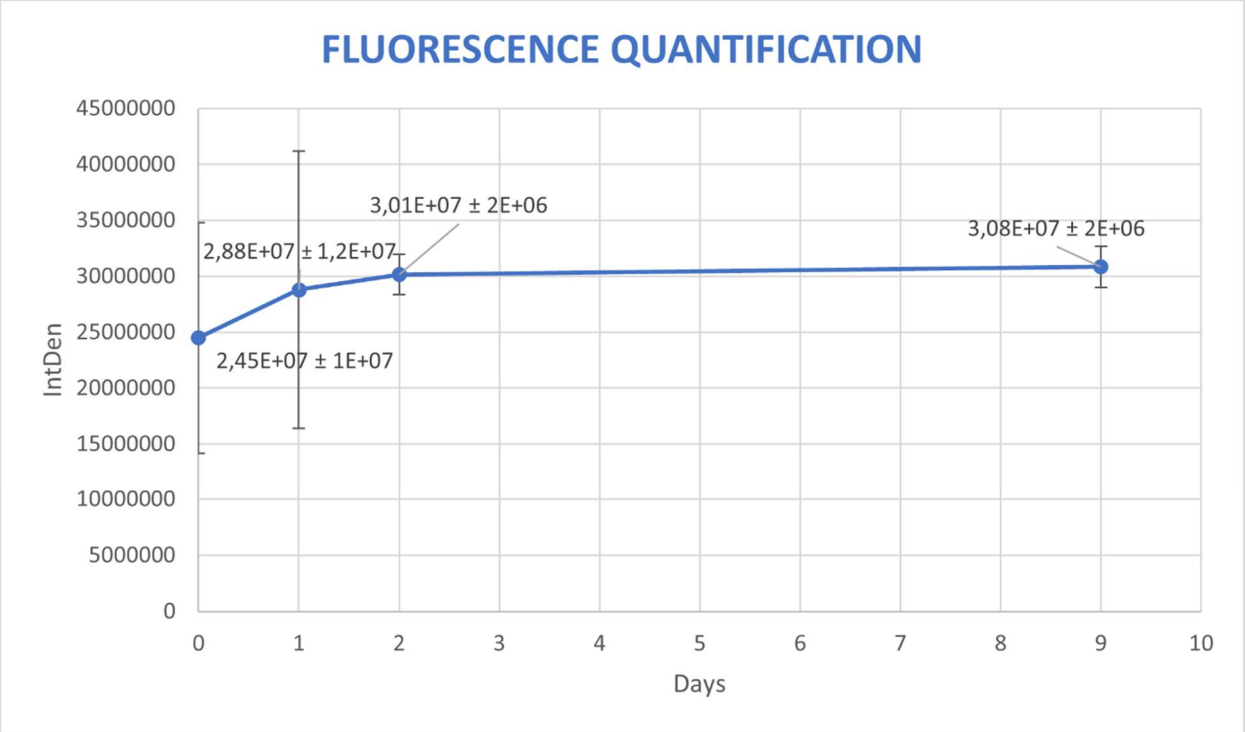

Figure 3.18 Graph of the fluorescence intensity (IntDen) along the culture days (from day 0 to 9)

This graph in fact allows to see an initial slow raise in fluorescence intensity, followed by a stabilization phase in which an almost constant value is reached. It should be further highlighted that fluorescence intensity is one order of magnitude lower than the previous experiment, proof that vital cells number is much lower.

Then, another experiment was performed with the purpose of overcoming the bioink viscosity hurdle and evaluate again cell distribution and vitality inside the constructs. This time GelMA C was mixed again with HUVEC GFP cells replicating the same density ($1.12*10^6$ cells/ml). In this case initial cells number was slower ($0.51*10^6$cells), a half the HUVECs number of the previous time, symptom of the fact that cells had reached a too high passage number decreasing their proliferation rate.

Furthermore, since room temperature was again higher (29°C) than the recommended 20-25°C, GelMA C cartridge was left in the incubator for only 10 min, then, after the mixing with cells, was left under the fume hood to reach room temperature (lower than 37°C) for 20 min and after that was put in the fridge for 10 min.

This allowed the bioink to be a little less liquid and thus to print the same 5 grids in a 6-wells plate with a pressure of 8 KPa. After 5 min-cooling, grids were photocured for 1 min, macroscopic and fluorescent images were captured (day 0), constructs were covered with culture medium (3 ml per well) and the 6-wells plate was incubated.

Even in this case the grids did not have the desired shape, but were warped, however at least were better than the previous case. Image acquisition lasted about 15 days (day 1, 5, 7, 9, 14) (Figure 3.19), during which the bioink structures, although they were misshaped, succeeded in maintaining their consistency without dissolving in the culture medium. Cells remained entrapped in bioink filaments without migrating towards the outer space and no contamination occurred.

Fluorescence images allowed to see a first increase in cells number and fluorescence intensity, synonym of cell proliferation, that than continued until it started to diminish, probably because of cell death.

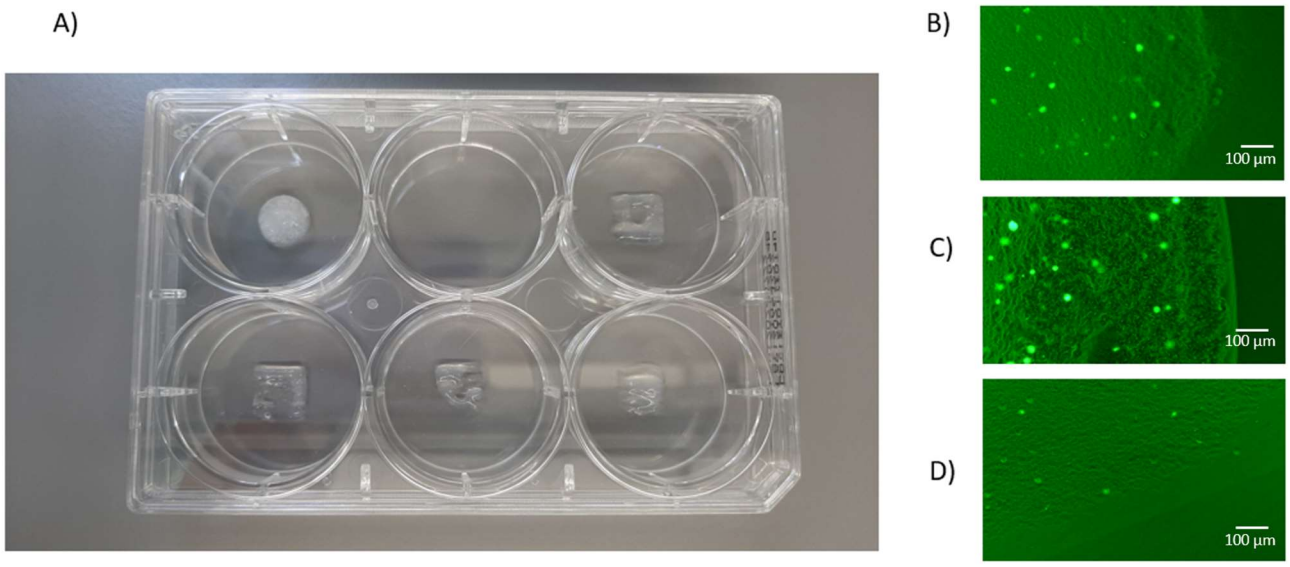

Figure 3.19 Macroscopic images of the printed grids on day 5 (A) and fluorescence microscopy images of the grid filaments on day 0 (B), day 9 (C) and day 14 (D)

These suppositions were validated by fluorescence quantification data (Figure 3.20).

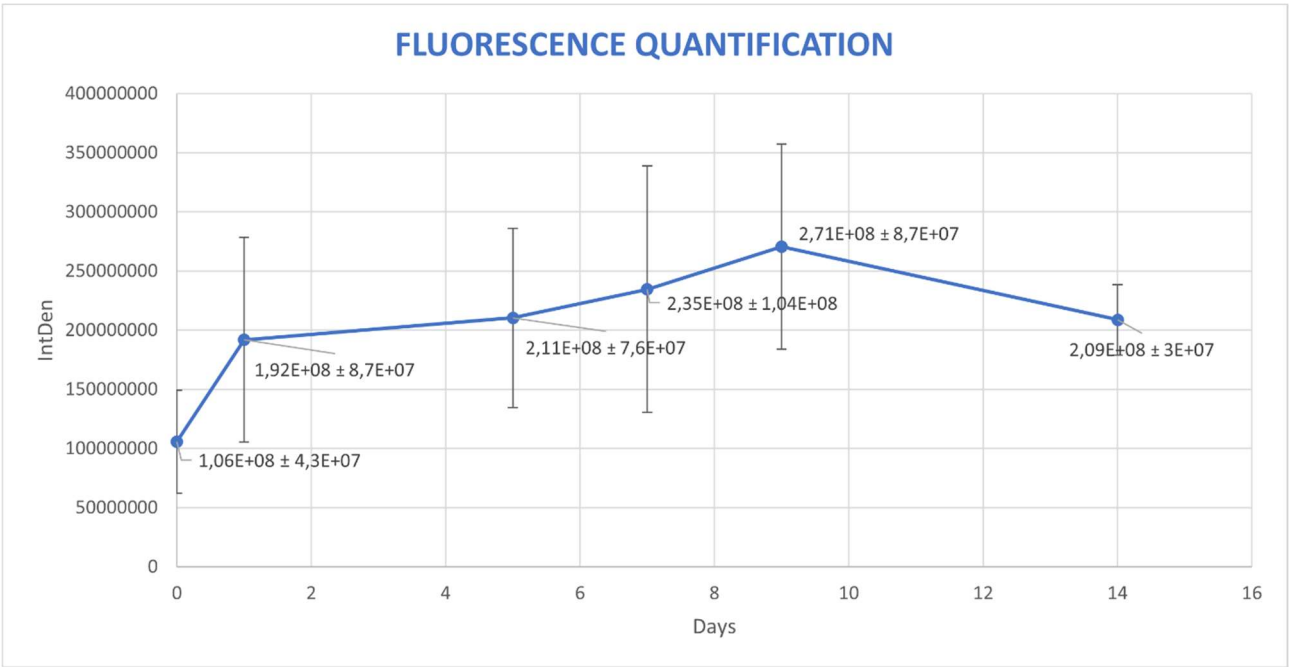

Figure 3.20 Graph of the fluorescence intensity (IntDen) along the culture days (from day 0 to 14)

The curve indeed displays an initial growth in fluorescence intensity, which later becomes slower, then a maximum is reached and eventually a decrease occurs. Unlike the previous experiment, fluorescence intensity is the same order of magnitude of the previous experiment with HUVECs,

but this time the values are lower compared to those of that experiment (the higher value is halved), partly because of the bioprinting process, which was not that optimal, but also because HUVECs cells were too old to proliferate.

Although protocol changes allowed to print a less liquid bioink, results were not the optimum and other adjustments had to be made. Moreover, HUVECs cells were too aged and thus were substituted with H5V GFP cells in the following experiment. GelMA bioink was mixed with these cells with the same cell density as before.

This time room temperature was even higher (32°C) and thus the protocol was further modified: first of all, GelMA C cartridge was left in the incubator for only 5 min, then, after being mixed with cells, it was left at room temperature for 15 min and lastly was put in the fridge for 20 min. Moreover, this time printhead was not preheated to 26°C to avoid additional heat source.

Although these changes, the bioink was still very liquid and the same 5 grids were printed in a 6-wells plate with a very low pressure, namely 2 KPa, to obtain a sufficiently thin filament. Since the bioink was that liquid, after 5 min-cooling in fridge, grids were crosslinked using again the 405 nm photocuring module, but this time for 2 min to assure bioink polymerization and avoid dissolution. After macroscopic and fluorescent images acquisition (day 0), culture medium was added (3 ml per well) to prevent cell dehydration and the 6-wells plate was put in the incubator.

Protocol adjustments allowed to print very well-shaped grids with a high resolution and shape fidelity (Figure 3.21), made up of low spreading and uniform thin filaments which didn't dissolve in the warm medium, but kept cells inside.

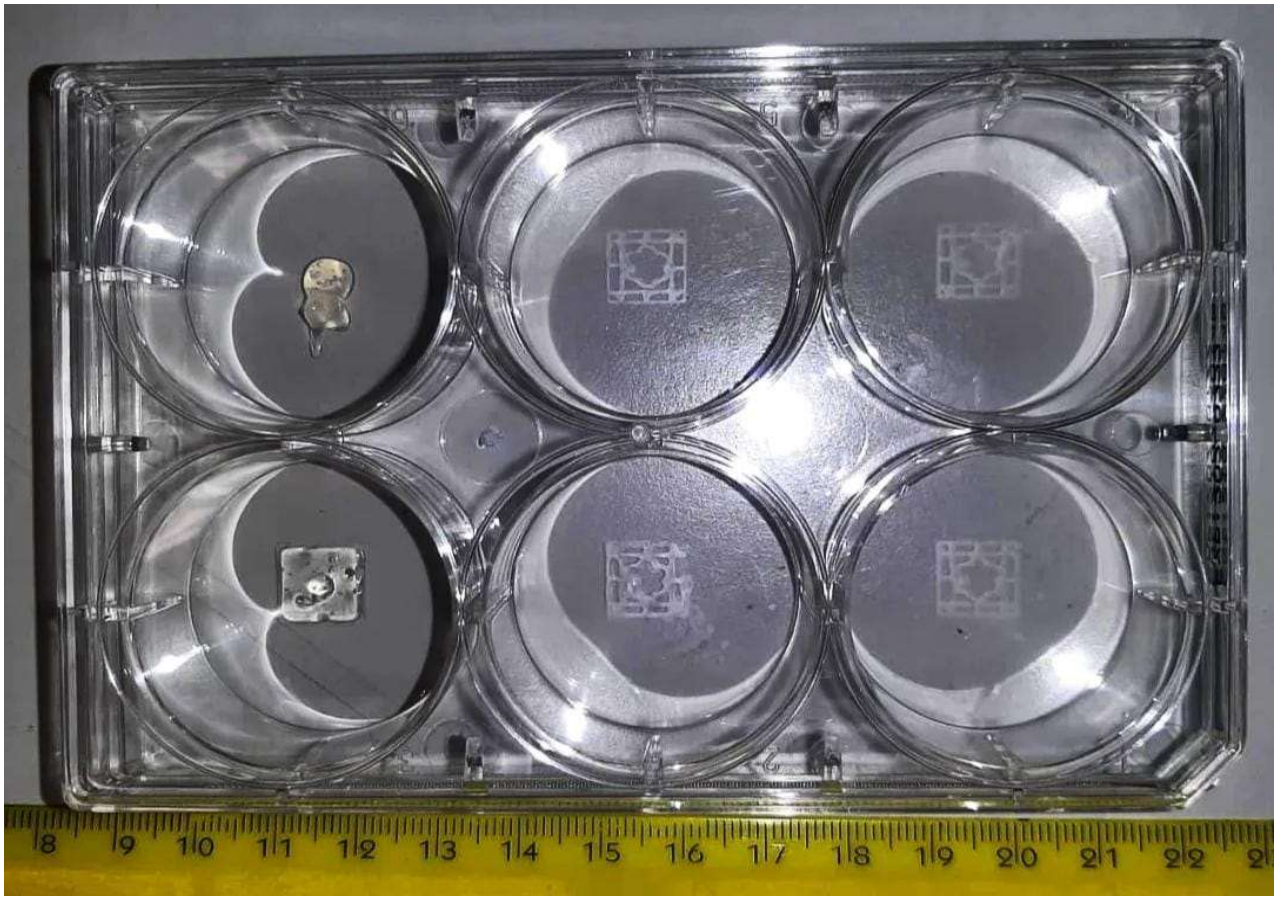

Figure 3.21 Grids printed using GelMA C bioink mixed with H5V GFP cells

In order to have a control, exactly the same procedure was repeated for the bioink without cells, with the precaution of letting the bioink at room temperature after the incubator for 30 min (instead of 15) to replicate also the time spent mixing the bioink with cells.

Thanks to the low pressure the printed grids were really accurate also in this case (Figure 3.22), but at the same time the bioink was equally very liquid, excluding the hypothesis of a possible influence of cell suspension on the overall viscosity.

Figure 3.22 Grids printed using GelMA C bioink alone

After grids printing, next step was to fill the flower-like holes with Caco2 cells-laden Matrigel droplets. Caco2 cells were resuspended in Matrigel with a cell density of 10^5 cells/ml and, after medium removal, every central grid hole was filled with a 10 µl-drop (Figure 3.23). This procedure was performed rapidly and keeping Matrigel eppendorf into crushed ice to avoid its gelation before being dispensed in the grids. After 30 min of incubation required for Matrigel polymerization, bright field images were acquired and eventually all the constructs were covered with warm culture medium. This procedure was carried out for both the grids with and without H5V cells to see the influence of the endothelial cells over Caco2 cells behaviour.

Figure 3.23 Caco2 cells-laden Matrigel droplets dispended inside the grid holes

Since day 0 fluorescence microscopy revealed that endothelial cells entrapped in the grids had a very low fluorescence intensity, suggesting that they were suffering. The day after (day 1), in fact, cells were almost died, as shown by fluorescence intensity which was almost null (Figure 3.24). One of the possible causes was the too long permanence in the fridge, which however was necessary to print the bioink as a filament instead of droplets. Culture therefore lasted only 2 days due to cell death, preventing from quantifying fluorescence for a sufficiently long period, but even this time no contamination happened.

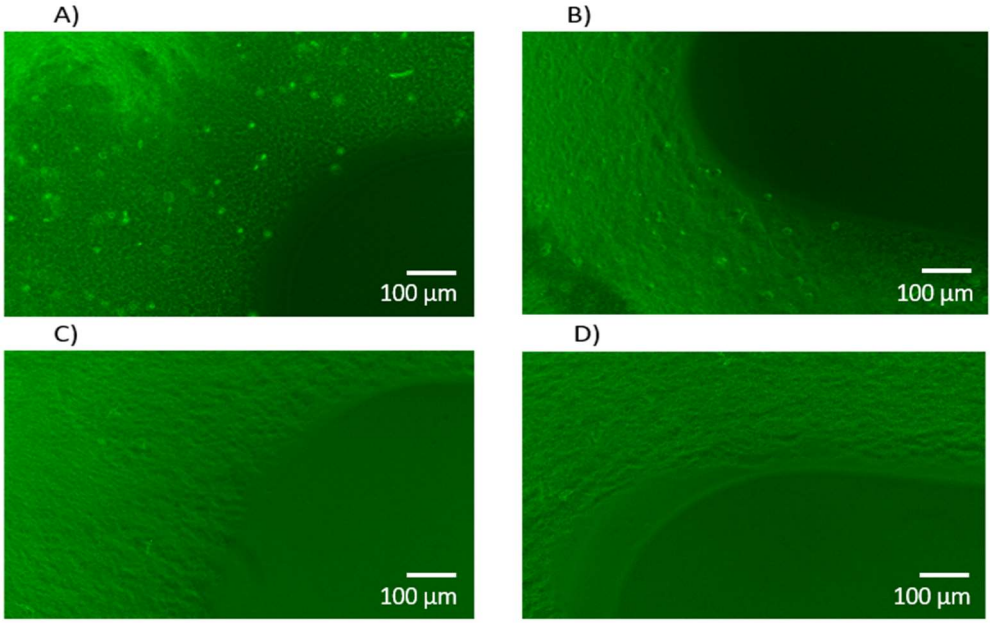

Figure 3.24 Fluorescence microscopy images of the grid filaments printed with GelMA C mixed with H5V GFP cells on day 0 (A) and day 1 (B) and without cells on day 0 (C) and day 1 (D)

As for the Caco2 cells images (Figure 3.25), in some cases cells were quite difficult to be found because of the many bubbles resulting from the reverse-forward pipetting of Matrigel to be mixed with cells, but also from Matrigel dispensing out of the 20 µl microtip. Moreover, the flower-like geometry was difficult to be correctly filled with Matrigel droplets, in fact in some parts there was a distance between the droplet and the grid, while in others an overlap of the two.

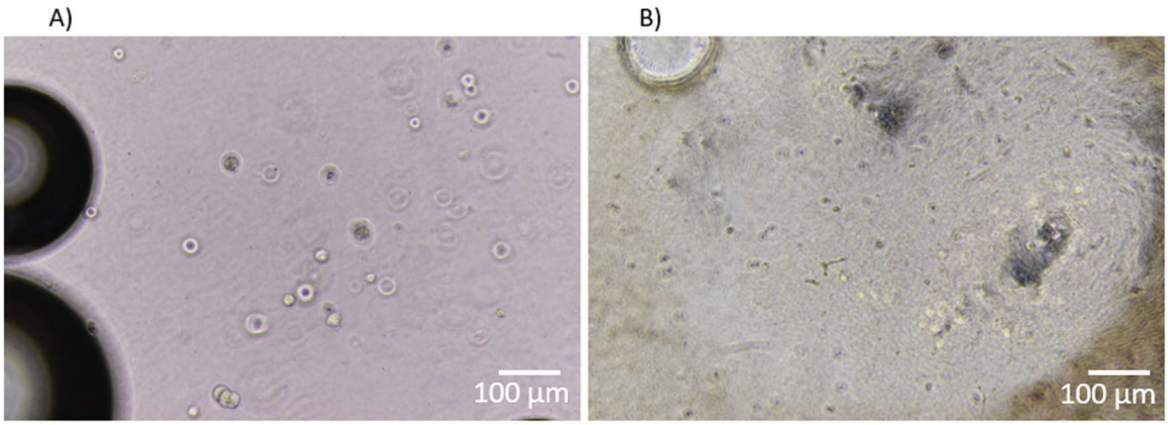

Figure 3.25 Brightfield microscopy images of Caco2 cells immersed in Matrigel on day 0 (A) and day 1 (B)

To simplify the experiment, which already had many issues to face, grids were modified substituting the flower-like hole with a 5 mm diameter-circular one (Figure 3.26).

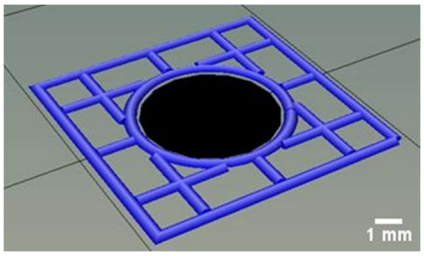

Figure 3.26 0.1 mm-high grid with a 5 mm-diameter circular hole

Even in this experiment the 5 modified grids were printed in 6-wells plates with both the bioink alone and the bioink mixed with cells. In the latter case H5V GFP cells were mixed with GelMA C replicating again the same cellular density.

With the attempt to overcome the previous hurdles, the protocol underwent other changes: first GelMA C cartridge was not placed in the incubator but was simply heated (from the fridge) leaving it under the biosafety cabined for 10 min, then it was mixed with cells and immediately after was put in the fridge for only 10 min (without being left at room temperature). Again the printhead was not preheated to 26°C and, additionally, two icepacks were positioned inside the printer chamber under the print bed (after being cleaned with 70% ethanol) to cool the print environment. Even in this case the same procedure was duplicated for the bioink alone, that was also left at room temperature before the fridge for 15 min, time required for the mixing with cells.

These modifications allowed to obtain a slightly more viscous bioink that was printed as a very thin filament with a higher pressure, i.e., 10 KPa, giving rise to precise and well-defined grids with a high shape fidelity in both cases with and without cells (Figure 3.27).

Although the slightly higher viscosity, grids underwent anyway photocuring for 2 min to assure bioink crosslinking and prevent dissolution in warm medium. After that, macroscopic and fluorescent images were acquired (day 0), structures were covered with culture medium (3 ml per well) to prevent cell dehydration and the 6-wells plates were incubated.

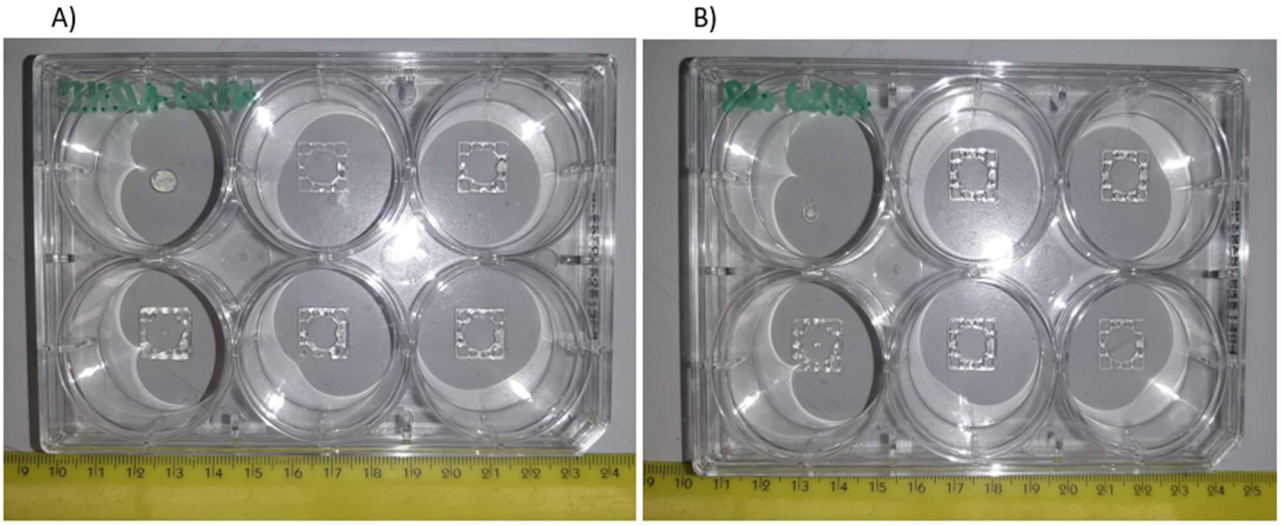

Figure 3.27 Grids printed using GelMA C bioink mixed with H5V GFP cells (A) and GelMA C bioink alone (B)

Then, Caco2 cells were resuspended in Matrigel replicating the same density (10^5 cells/ml) and a 10 µl-drop was placed in every circular hole of the grids. Then 6-well plates were incubated for 30 min for Matrigel gelation, bright field images were captured and lastly culture medium was added to cover the structures.

To avoid bubbles formation in Matrigel, in addition to the precaution of a really slow reverse-forward pipetting, 20 µl-microtips were frozen for the whole night before the experiment and this effectively allowed to significantly reduce the bubbles and thus to see the cells in bright-field microscopy (Figure 3.28). Moreover, the simplified geometry effectively helped the correct holes filling, without any overlap or empty space.

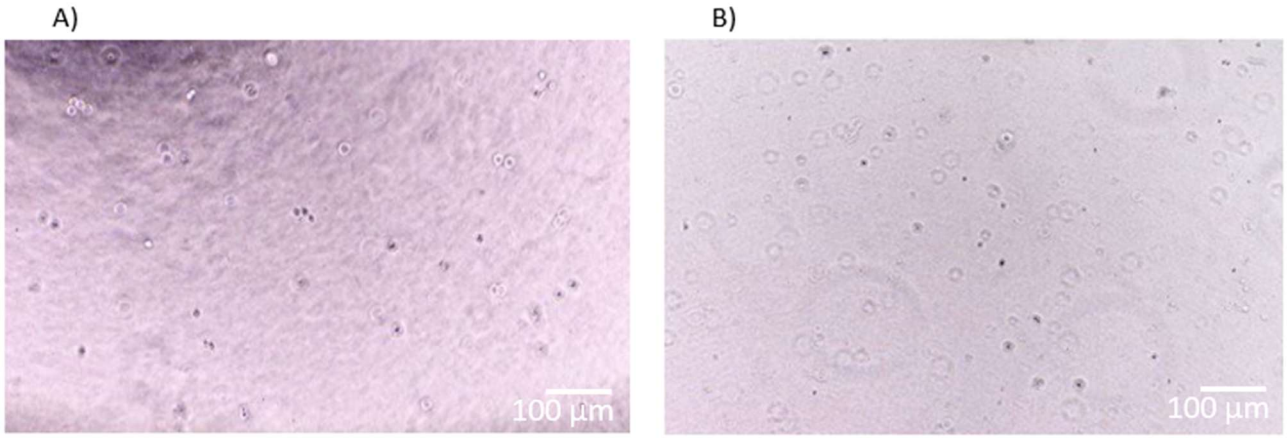

Figure 3.28 Brightfield microscopy images of Caco2 cells immersed in Matrigel on day 0 (A) and day 1 (B)

Although the protocol adjustments, included the halved time in fridge, florescence microscopy showed a really low fluorescence intensity also in this case, that on day 1 was even lower, suggesting that maybe 2 min-photocuring was too much for cell survival (Figure 3.29). Increasing the crosslinking time, therefore, did not prove to be the suitable strategy to overcome the bioink viscosity issue and, regrettably, in this case it might have been an unnecessary additional precaution. Unfortunately, it was not possible to assess whether this protocol accommodation, together with 1-min photocrosslinking, could effectively lead to a greater cell survival.

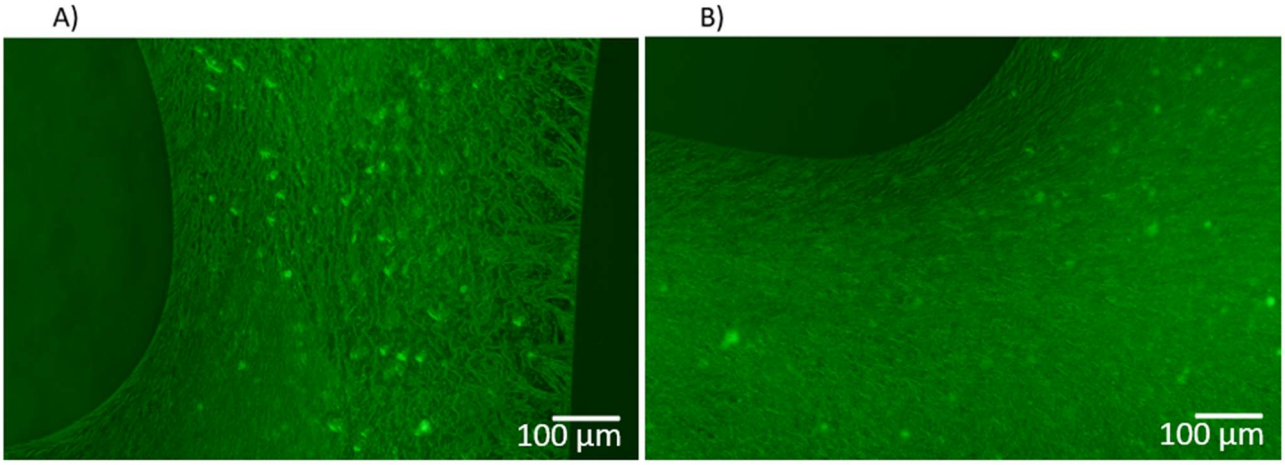

Figure 3.29 Fluorescence microscopy images of the grid filaments printed with GelMA C mixed with H5V GFP cells on day 0 (A) and day 1 (B)

4. Conclusions

Given the increasingly pressing need of *in vitro* models of human tissues, organoid technology seems to be gaining a larger and larger foothold in biomedical research allowing to overcome 2D cell cultures and animal models limitations.

Organoids are indeed 3D multicellular structures derived from human cells self-organization that recapitulate organ-specific architecture and functionality and therefore they represent a powerful human-specific model system that holds great promises for regenerative medicine, drug discovery and personalised medicine.

However, one of the main limitations in achieving completely functional organoids is the absence of a perfusing system that prevent them from growing up to the right size, surviving for long and, thus, maturing beyond the embryonic and fetal phase.

Many strategies for *in vitro* organoid vascularization are being studied, starting from pre-vascularization up to engineering of perfusable capillary beds, however, to date only *in vivo* transplantation into host animals has been proven to achieve tissue vascularization with complete function.

It is in this context that this master thesis fits, aiming to bioprint a vascular network intended to host and perfuse colon organoids. In particular, this work focused on the optimization of the whole bioprinting process of the network, starting from the definition of the lattice geometry and printing parameters, then moving on to the G-codes modification, up to the optimization of the out-and-out bioprinting process.

Preliminary studies allowed to determine the suitable printing parameters, namely the infill pattern and density of the lattice, the height of the constructs and the corresponding printing speeds. Then the different geometries of the structures to be printed were defined and optimized, both for the higher constructs intended to envelop organoids and the monolayer grids for cell imaging, including the geometries of the inner holes for both cases.

After that, different strategies to create and culture the vascular network with colon organoids right inside its cavity were established, from the simple lattice bioprinting with colon cells dispensing inside the hollow, to 2-step bioprinting and dual printhead bioprinting. In the latter two cases also the internal structures to be printed inside the holes were studied and optimized, but at the same time these two approaches turned out to also require some G-codes modifications that, eventually, enabled to succeed in printing both the inner and the outer structures without damaging each other. Moreover, G-code adjustments also allowed the simultaneous bioprinting of multiple constructs in a multi-well plate.

Concerning the real bioprinting process, although the several hurdles to overcome, many achievements were fulfilled. First of all, the bioprinting protocol was refined enabling to reduce air bubbles introduction as well as material waste, but also to maintain sterility for the entire procedure. The choice of the correct nozzle allowed to meet both good resolution and cell viability. Then the suitable bioink, in terms of printability and shape fidelity but also of transparency for cell imaging, was found. The selection of the adequate crosslinking wavelength and duration (1 min) enabled to prevent both constructs dissolution in culture medium and cell suffering, as evidenced by the results of the first HUVECs printing, that allowed the cells to proliferate and survive right inside the bioink filaments for about 20 days. Moreover, procedure optimization considerably reduced bubbles formation in Matrigel, making cells visible under the microscope. Furthermore, although all the various criticalities of such a challenging process, thanks to the adaptation of the protocol it was possible to bioprint high-resolution constructs that did not dissolve even in non-optimal environmental conditions.

However, such good results were achieved keeping the extra precaution of a longer photocuring (2 min), that unfortunately caused cell death and which might have been unnecessary. Regrettably, it could not be verified whether the protocol adjustments, together with the correct crosslinking duration (1 min), could effectively yield good results also in terms of cell viability. This was one of the main limits of the present work, but it was actually related to the environmental conditions that ultimately affected bioink viscosity. In fact, as already stated, good result in terms of printability and cell survival and growth could be reached with an optimal room temperature.

Another drawback of the present work was related to the 3D printer resolution (which depends on the nozzle size, printing speed and pressure), that does not enable to print filaments with an even smaller diameter that may better mimic that of *in vivo* capillaries.

Furthermore, as already mentioned, to achieve a fully perfusable system a vascular bed is not enough, but an *in vitro* pre-vascularization, followed by the anastomosis between external vessels and internal vasculature, would be crucial. Therefore, the following step of this work could be the co-colture of Caco2 cells together with endothelial cells to create pre-vascularized organoids right inside the lattice hollows and then anastomose the internal vessels with the printed vascular network.

Obviously prior to this, further printings and characterizations are mandatory, as well as supporting fluorescence quantifications. Then, next step would be the bioprinting of all the other remaining

prepared constructs using the endothelial cells-laden bioink and the culture with colon cells-laden Matrigel droplets up to capillary and organoids formation. Moreover, the influence of such a network on organoids growth should be evaluated in all the different cases. Additionally, confocal microscopy could be used to detect cells in multi-layered constructs. After that, also 2-step and dual printheads bioprintings should be experimented with cells.

Last but not least, although this thesis has focused on colon organoids, geometry changes could be carried out to adapt this vascular network to the vascularization of a different kind of organoids.

References

[1] C. Corrò, L. Novellasdemunt, and V. S. W. Li, "A brief history of organoids," *Am J Physiol Cell Physiol*, vol. 319, no. 1, pp. C151–C165, Jul. 2020, doi: 10.1152/ajpcell.00120.2020.

[2] M. Kapałczyńska *et al.*, "2D and 3D cell cultures – a comparison of different types of cancer cell cultures," *Archives of Medical Science*, vol. 14, no. 4, pp. 910–919, 2018, doi: 10.5114/aoms.2016.63743.

[3] J. Kim, B. K. Koo, and J. A. Knoblich, "Human organoids: model systems for human biology and medicine," *Nature Reviews Molecular Cell Biology*, vol. 21, no. 10. Nature Research, pp. 571–584, Oct. 01, 2020. doi: 10.1038/s41580-020-0259-3.

[4] S. Zhang, Z. Wan, and R. D. Kamm, "Vascularized organoids on a chip: strategies for engineering organoids with functional vasculature," *Lab on a Chip*, vol. 21, no. 3. Royal Society of Chemistry, pp. 473–488, Feb. 07, 2021. doi: 10.1039/d0lc01186j.

[5] C. S. Hughes, L. M. Postovit, and G. A. Lajoie, "Matrigel: a complex protein mixture required for optimal growth of cell culture.," *Proteomics*, vol. 10, no. 9, pp. 1886–1890, 2010, doi: 10.1002/pmic.200900758.

[6] "Technologies for Regenerative Medicine notes." 2021.

[7] S. Rahmani, N. M. Breyner, H. M. Su, E. F. Verdu, and T. F. Didar, "Intestinal organoids: A new paradigm for engineering intestinal epithelium in vitro," *Biomaterials*, vol. 194. Elsevier Ltd, pp. 195–214, Feb. 01, 2019. doi: 10.1016/j.biomaterials.2018.12.006.

[8] H. Clevers, "Modeling Development and Disease with Organoids," *Cell*, vol. 165, no. 7. Cell Press, pp. 1586–1597, Jun. 16, 2016. doi: 10.1016/j.cell.2016.05.082.

[9] "Bioreactors notes," *2021*.

[10] A. Vargas-Valderrama, A. Messina, M. T. Mitjavila-Garcia, and H. Guenou, "The endothelium, a key actor in organ development and hPSC-derived organoid vascularization," *Journal of Biomedical Science*, vol. 27, no. 1. BioMed Central Ltd., May 22, 2020. doi: 10.1186/s12929-020-00661-y.

[11] X. Zhao *et al.*, "Review on the Vascularization of Organoids and Organoids-on-a-Chip," *Frontiers in Bioengineering and Biotechnology*, vol. 9. Frontiers Media S.A., Apr. 12, 2021. doi: 10.3389/fbioe.2021.637048.

[12] A. Dellaquila, C. le Bao, D. Letourneur, and T. Simon-Yarza, "In Vitro Strategies to Vascularize 3D Physiologically Relevant Models," *Advanced Science*, vol. 8, no. 19. John Wiley and Sons Inc, Oct. 01, 2021. doi: 10.1002/advs.202100798.

[13] Y. Ze *et al.*, "Three-dimensional bioprinting: A cutting-edge tool for designing and fabricating engineered living materials," *Biomaterials Advances*, vol. 140, Sep. 2022, doi: 10.1016/j.bioadv.2022.213053.

[14] M. Dey and I. T. Ozbolat, "3D bioprinting of cells, tissues and organs," *Scientific Reports*, vol. 10, no. 1. Nature Research, Dec. 01, 2020. doi: 10.1038/s41598-020-70086-y.

[15] E. P. Chen, Z. Toksoy, B. A. Davis, and J. P. Geibel, "3D Bioprinting of Vascularized Tissues for in vitro and in vivo Applications," *Frontiers in Bioengineering and Biotechnology*, vol. 9. Frontiers Media S.A., May 13, 2021. doi: 10.3389/fbioe.2021.664188.

[16] "骨组织工程支架 61打印系统的建立与支架宏微 结构精度的可控性评价."

[17] "Beginners Guide to 3D Printing G-Code Commands | Simplify3D." https://www.simplify3d.com/support/articles/3d-printing-gcode-tutorial/ (accessed Sep. 05, 2022).

[18] A. N. Leberfinger *et al.*, "Bioprinting functional tissues," *Acta Biomaterialia*, vol. 95. Acta Materialia Inc, pp. 32–49, Sep. 01, 2019. doi: 10.1016/j.actbio.2019.01.009.

[19] "INKREDIBLE+ User manual."

[20] "INKREDIBLE+ 3D Bioprinter - CELLINK." https://www.cellink.com/bioprinting/inkredible-3d-bioprinter/ (accessed Sep. 05, 2022).

[21] "SolidWorks: 3D Modeling Software with parametric construction." https://www.sculpteo.com/en/glossary/solidworks-definition/ (accessed Sep. 05, 2022).

[22] "SolidWorks - Wikipedia." https://en.wikipedia.org/wiki/SolidWorks (accessed Sep. 05, 2022).

[23] "PrusaSlicer | Original Prusa 3D printers directly from Josef Prusa." https://www.prusa3d.com/page/prusaslicer_424/ (accessed Sep. 05, 2022).

[24] "Creating profiles for different nozzles | Prusa Knowledge Base." https://help.prusa3d.com/article/creating-profiles-for-different-nozzles_127540 (accessed Sep. 05, 2022).

[25] "2.2.22. Post-processing PrusaSlicer G-Code — Bob's Project Notebook." https://projects.ttlexceeded.com/3dprinting_prusaslicer_post-processing.html (accessed Sep. 05, 2022).

[26] "Spyder (software) - Wikipedia." https://en.wikipedia.org/wiki/Spyder_(software) (accessed Sep. 05, 2022).

[27] "EA.hy926 - CRL-2922 | ATCC." https://www.atcc.org/products/crl-2922 (accessed Sep. 05, 2022).

[28] "EAhy 926 cell." https://www.ebi.ac.uk/ols/ontologies/efo/terms?short_form=EFO_0003039 (accessed Sep. 05, 2022).

[29] "Immortalized Human Vascular Endothelial Cells (EA.hy926)." https://www.abmgood.com/immortalized-human-vascular-endothelial-cells-ea-hy926.html (accessed Sep. 05, 2022).

[30] "EA.hy926 | APABCAM." https://bcrj.org.br/celula/ea-hy926-endotelial-human (accessed Sep. 05, 2022).

[31] "Primary Umbilical Vein Endothelial Cells; Normal, Human (HUVEC) - PCS-100-010 | ATCC." https://www.atcc.org/products/pcs-100-010 (accessed Sep. 05, 2022).

[32] "Human Umbilical Vein Endothelial Cells, HUVEC Cells | Molecular Devices." https://www.moleculardevices.com/applications/cell-counting/cell-counter-huvec-cells#gref (accessed Sep. 05, 2022).

[33] "HEK293-GFP-stable-cell." https://www.cellomicstech.com/product/1681/hek293gfp-cmv-stable-cells (accessed Sep. 05, 2022).

[34] "HEK293, cellule HEK293-GFP, cellule HEK | Molecular Devices." https://it.moleculardevices.com/applications/cell-counting/cell-counter-hek293-gfp-cells#gref (accessed Sep. 05, 2022).

[35] C. Garlanda *et al.*, "Progressive growth in immunodeficient mice and host cell recruitment by mouse endothelial cells transformed by polyoma middle-sized T antigen: Implications for the pathogenesis of opportunistic vascular tumors (hemangloma/secondary lesion/nude mice)," 1994. [Online]. Available: https://www.pnas.org

[36] "Cellosaurus cell line H5V (CVCL_AZ87)." https://www.cellosaurus.org/CVCL_AZ87 (accessed Sep. 05, 2022).

[37] "Caco-2 [Caco2] - HTB-37 | ATCC." https://www.atcc.org/products/htb-37 (accessed Sep. 05, 2022).

[38] "Caco-2 - Wikipedia." https://en.wikipedia.org/wiki/Caco-2 (accessed Sep. 05, 2022).

[39] T. Lea, "Caco-2 cell line," in *The Impact of Food Bioactives on Health: In Vitro and Ex Vivo Models*, Springer International Publishing, 2015, pp. 103–111. doi: 10.1007/978-3-319-16104-4_10.

[40] "CELLINK FIBRIN - CELLINK." https://www.cellink.com/product/cellink-fibrin/ (accessed Sep. 05, 2022).

[41] "Specification Sheet." [Online]. Available: www.cellink.com

[42] "GelMA C - CELLINK." https://www.cellink.com/product/gelma-c/ (accessed Sep. 05, 2022).

[43] "Specification Sheet." [Online]. Available: www.cellink.com

[44] "Matrigel - Wikipedia." https://en.wikipedia.org/wiki/Matrigel (accessed Sep. 05, 2022).

[45] "Matrigel® Basement Membrane Matrix | VWR." https://it.vwr.com/store/product/en/826102/matrice-della-membrana-di-base-corning-matrigel?languageChanged=en (accessed Sep. 05, 2022).

[46] "Corning® Matrigel® Matrix | Everything You Ever Wanted to Ask | Corning." https://www.corning.com/in/en/products/life-sciences/resources/stories/at-the-bench/everything-you-ever-wanted-to-ask-about-corning-matrigel-matrix.html (accessed Sep. 05, 2022).

[47] "Background 1. What is Corning Matrigel matrix? Amounts of Growth Factors (GF) Present in Corning Matrigel Matrix vs. Growth Factor Reduced (GFR) Corning Matrigel Matrix Growth Factor Range of GF Concentration in Corning Matrigel Matrix Average GF

Concentration in Corning Matrigel Matrix Typical GF Concentration in GFR Corning Matrigel Matrix Corning ® Matrigel ® Matrix Frequently Asked Questions."

[48] "What is the proper storage temperature of Matrigel® matrix?" https://cellculturedish.com/questions/what-is-the-proper-storage-temperature-of-matrigel-matrix/ (accessed Sep. 05, 2022).

[49] H. K. Kleinman and G. R. Martin, "Matrigel: Basement membrane matrix with biological activity," *Seminars in Cancer Biology*, vol. 15, no. 5 SPEC. ISS. Academic Press, pp. 378–386, 2005. doi: 10.1016/j.semcancer.2005.05.004.

[50] "NIS-Elements Microscope Imaging Software | NIS Software | Nikon Metrology." https://www.nikonmetrology.com/en-us/industrial-microscopes/nis-software-nis-elements-microscope-imaging-software (accessed Sep. 05, 2022).

[51] "NIS-Elements.cz (Laboratory Imaging)." https://www.nis-elements.cz/en (accessed Sep. 05, 2022).

[52] "ImageJ - Wikipedia." https://en.wikipedia.org/wiki/ImageJ (accessed Sep. 05, 2022).

[53] R. Csepregi, V. Temesf oi, M. Poór, Z. Faust, and T. K oszegi, "Green fluorescent protein-based viability assay in a multiparametric configuration," *Molecules*, vol. 23, no. 7, 2018, doi: 10.3390/molecules23071575.

[54] "Bioprinting-Protocol-CELLINK-FIBRIN_-21-June-2021".

[55] GelMA C, "Bioprinting Protocol Materials needed-GelMA C bioink*-UV shielding cartridges, 3cc*-Sterile Conical Bioprinting nozzles, 22-27G*-BIO X*, BIO X6* or INKREDIBLE+* 3D Bioprinters-405 or 365 nm UV modules for photocuring-Cells + cell culture medium-3 mL syringes with Luer lock connections-Female/female Luer lock adaptor*-CELLMIXER*," 2021. [Online]. Available: www.cellink.com

[56] "Mixing-cells-Protocol-GelMA-series_22-July-2021".

[57] "Photocrosslinking Optimization Protocol." [Online]. Available: www.cellink.com|+1

[58] J. L. Dávila, B. M. Manzini, M. A. d'Ávila, and J. V. L. da Silva, "Open-source syringe extrusion head for shear-thinning materials 3D printing," *Rapid Prototyp J*, 2022, doi: 10.1108/RPJ-09-2021-0245.

[59] N. Paxton, W. Smolan, T. Böck, F. Melchels, J. Groll, and T. Jungst, "Proposal to assess printability of bioinks for extrusion-based bioprinting and evaluation of rheological properties governing bioprintability," *Biofabrication*, vol. 9, no. 4, Nov. 2017, doi: 10.1088/1758-5090/aa8dd8.

[60] J. C. Gómez-Blanco, E. Mancha-Sánchez, A. C. Marcos, M. Matamoros, A. Díaz-Parralejo, and J. B. Pagador, "Bioink temperature influence on shear stress, pressure and velocity using computational simulation," *Processes*, vol. 8, no. 7, Jul. 2020, doi: 10.3390/PR8070865.

[61] E. Reina-Romo, S. Mandal, P. Amorim, V. Bloemen, E. Ferraris, and L. Geris, "Towards the Experimentally-Informed In Silico Nozzle Design Optimization for Extrusion-Based Bioprinting of Shear-Thinning Hydrogels," *Front Bioeng Biotechnol*, vol. 9, Aug. 2021, doi: 10.3389/fbioe.2021.701778.

[62] D. Richards, J. Jia, M. Yost, R. Markwald, and Y. Mei, "3D Bioprinting for Vascularized Tissue Fabrication," *Annals of Biomedical Engineering*, vol. 45, no. 1. Springer New York LLC, pp. 132–147, Jan. 01, 2017. doi: 10.1007/s10439-016-1653-z.